

2019-09-12

Sediment and organic carbon transport and deposition driven by internal tides along Monterey Canyon, offshore California

Maier, KL

<http://hdl.handle.net/10026.1/14928>

10.1016/j.dsr.2019.103108

Deep Sea Research Part I: Oceanographic Research Papers

Elsevier

All content in PEARL is protected by copyright law. Author manuscripts are made available in accordance with publisher policies. Please cite only the published version using the details provided on the item record or document. In the absence of an open licence (e.g. Creative Commons), permissions for further reuse of content should be sought from the publisher or author.

**Sediment and organic carbon transport and deposition driven by internal tides
along Monterey Canyon, offshore California**

Katherine L. Maier^{1,2*}, Kurt Rosenberger², Charles K. Paull¹, Roberto Gwiazda¹, Jenny Gales³, Thomas Lorenson², James P. Barry¹, Peter J. Talling⁴, Mary McGann⁵, Jingping Xu⁶, Eve Lundsten¹, Krystle Anderson¹, Steven Y. Litvin¹, Daniel R. Parsons⁷, Michael A. Clare⁸, Stephen M. Simmons⁷, Esther J. Sumner⁹, Matthieu J. Cartigny⁴

¹Monterey Bay Aquarium Research Institute, 7700 Sandholdt Road, Moss Landing, California, 95039 USA

²U.S. Geological Survey, Pacific Coastal and Marine Science Center, 2885 Mission Street, Santa Cruz, California, 95060 USA

³University of Plymouth, Drake Circus, Plymouth, Devon, PL4 8AA UK

⁴Durham University, Departments of Geography and Earth Sciences, Lower Mountjoy, South Road, Durham, DH1 3LE UK

⁵U.S. Geological Survey, Pacific Coastal and Marine Science Center, 345 Middlefield Road, MS999, Menlo Park, California, 94025 USA

⁶Southern University of Science and Technology of China, Department of Ocean Science and Engineering, No 1088, Xueyuan Rd., Nanshan District, Shenzhen, Guangdong, China

⁷University of Hull, Energy and Environment Institute, Hull, HU6 7RX UK

⁸National Oceanography Centre, European Way, Southampton, SO14 3ZH UK

⁹University of Southampton, Ocean and Earth Science, University Road, Southampton, SO17 1BJ UK

*corresponding author: Katie.Maier@niwa.co.nz

present affiliation: National Institute of Water and Atmospheric Research, Wellington, New Zealand

ABSTRACT

Submarine canyons are globally important conduits for sediment and organic carbon transport into the deep sea. Using a novel dataset from Monterey Canyon, offshore central California, that includes an extensive array of water column sampling devices, we address how fine-grained sediment and organic carbon are transported, mixed, fractionated, and buried along a submarine canyon. Anderson-type sediment traps were deployed 10 to 300 meters above the seafloor on a suite of moorings anchored between 278–1849 m water depths along the axial channel of Monterey Canyon during three consecutive 6-month deployments (2015–2017). Tidal currents within the canyon suspended and transported fine-grained sediment and organic carbon that were captured in sediment traps, which record the composition of sediment and organic carbon transport along the canyon. High sediment accumulation rates in traps increased up-canyon and near the seafloor, where fine-scale (<1 cm) layering was increasingly distinctive in CT scans. There was no along-canyon trend in the organic carbon composition (percent modern carbon and isotopic signatures) among trap locations, suggesting effective mixing. Organic carbon content (weight percent total organic carbon) and excess ^{210}Pb activities (dpm/g) increased down-canyon, reflecting reduced flux of sediment and organic carbon into deeper water, more distal traps. Differing organic carbon signatures in traps compared with previous measurements of seabed deposits along Monterey Canyon suggest that organic carbon transported through the canyon with internal tides may not be consistently recorded in seafloor deposits. First-order estimates from comparing organic carbon content of core and trap samples results in low organic carbon specific burial efficiency (ranging from ~26% to ~0.1%) and suggests that the modern upper Monterey Canyon may not be an effective sink for carbon. Organic carbon isotopic signatures from sediment traps in the water column show more marine influence than seafloor sediment cores; this is likely due to the deposition and reworking of seafloor deposits by sediment density flows and preferential consumption of fresh marine organic carbon on the seafloor, which is better preserved in the traps. Sediment and remaining organic carbon in canyon floor and lower flank deposits preferentially reflect episodic sediment density flow events that are unrelated to internal tides. This study provides a quantified example and conceptual model for internal-tide-related sediment and organic carbon transport, mixing, and burial trends along a submarine canyon that are likely to be similar in many canyons worldwide.

Keywords (4–6): submarine canyon; sediment trap; internal tide; organic carbon; xs^{210}Pb

1. Introduction

Submarine canyons are globally important as conduits for offshore transport of sediment and organic carbon, as dynamic areas of ocean mixing, and as biodiversity hotspots (e.g., Shepard, 1979; Hotchkiss and Wunsch, 1982; Harris and Whiteway, 2011; Talling et al., 2015; Amaro et al., 2016; Liao et al., 2017; Mountjoy et al., 2018). These canyon systems funnel terrestrial- and marine-sourced organic carbon into the deep-sea, feeding deep-sea ecosystems within and beyond canyon environments (e.g., Amaro et al., 2015; Baudin et al., 2017; Liao et al., 2017; Campanyà-Llovet et al., 2018). A fraction of organic carbon in these deep-sea conduits is buried and contributes to global carbon biogeochemical cycling and atmospheric carbon dioxide levels over time (e.g., Galy et al., 2007; Masson et al., 2010; Zheng et al., 2017; Mountjoy et al., 2018). Comprehensive direct sampling of submarine canyon deep-sea environments is needed to more fully elucidate the geological, ecological, and oceanographic role of submarine canyons over time.

The transport of sediment and organic matter along submarine canyons can occur in sediment density flows and internal tidal flows. Episodic turbidity currents and other sediment density flow events can move vast amounts of sediment into deeper water and rapidly alter the seafloor on the scale of meters to tens of meters in a single event (e.g., Talling et al., 2015; Mountjoy et al., 2018; Paull et al., 2018; Vendettouli et al., 2019). Between sediment density flow events, submarine canyons can focus internal wave energy, creating internal tidal flows that transport, erode, and inhibit deposition of fine-grained sediment (e.g., Shepard and Marshall, 1969; Shepard, 1976, 1979; Gardner, 1989; Petruncio et al., 1998; Cacchione et al., 2002; Carter and Gregg, 2002; Xu et al., 2002b; Lee et al., 2009; Xu and Noble, 2009; Wain et al., 2013; Waterhouse et al., 2017; Li et al., 2019). Herein, we refer to internal tides generally as internal waves with tidal frequencies, after Pomar et al. (2012).

Monterey Canyon, offshore central California (Fig. 1), is one of the most studied submarine canyons on Earth (e.g., Matos et al., 2018) and has been a focus of studies on canyon sediment transport processes, as well as depositional facies, for many years (e.g., Paull et al., 2003, 2010a, 2011, 2018; Smith et al., 2005, 2007; Xu et al., 2002b, 2014; Stevens et al., 2014; Symons et al., 2017; Maier et al., 2019). Episodic sediment density flow events occur in Monterey Canyon with sub-annual frequency, and semi-diurnal internal tides have been measured to 3300 meters water depth along the canyon-channel axis (e.g., Xu and Noble, 2009; Paull et al., 2010a, 2018). Xu and Noble (2009) documented internal tidal variation in Monterey Canyon being offset from the sea surface semi-diurnal tide and noted that internal tidal flows may prevent Monterey Canyon axis from infilling with fine-grained sediment. Internal tidal flows in Monterey Canyon have been measured with speeds of 20–80 cm/s and are an order of magnitude larger than open ocean tidal currents (e.g., Petruncio et al., 1998; Kunze et al., 2002). Internal tides appear to be generated from seafloor topography offshore central California, in and around

Monterey Canyon (e.g., Petruncio et al., 1998, 2002; Kunze et al., 2002; Hall and Carter, 2011). Internal tidal velocities increase up-canyon, enhanced by the slope of the canyon floor (1.7° , Paull et al., 2005) and headward narrowing of the canyon (Fig. 1) (e.g., Hotchkiss and Wunsch, 1982; Petruncio et al., 1998, 2002; Carter and Gregg, 2002).

An international collaborative effort was developed to comprehensively instrument Monterey Canyon and address the need for detailed direct measurements of submarine canyon sediment transport (Paull et al., 2018). This novel experiment, referred to as the Coordinated Canyon Experiment (CCE), was designed primarily to measure sediment density flow events (Paull et al., 2018). The resulting dataset provides the most detailed monitoring yet of a submarine canyon, including 15 sediment density flow events (criteria detailed in Paull et al., 2018) during 18 months of high-frequency water column measurements and sediment samples, collected during and between sediment density flow events (Paull et al., 2018; Maier et al., 2019). Specifically, the CCE array included an unprecedented number of sediment traps deployed in close proximity to the seafloor, allowing analysis of submarine canyon sediment transport and organic carbon down 50 km of the canyon axis on moorings anchored at 278 to 1849 meters water depth (Figs. 1, 2).

In this study, our primary aim is to investigate how sediment and organic carbon are transported, mixed, and preserved within a submarine canyon, specifically focusing on samples from intervals between sediment density flow events that represent most of the CCE study time period. For these intervals not associated with sediment density flow events, we compare organic carbon content and composition sampled directly from the water column in sediment traps with results from previously analyzed (Paull et al., 2006) samples of seafloor sediments. We address three interrelated questions: (1) How are fine-grained sediment and organic carbon transported in a submarine canyon between sediment density flow events? (2) How is organic carbon fractionated and (or) mixed along the canyon? (3) How are transported (water column) organic carbon and fine-grained sediment preserved in canyon deposits? Results from Monterey Canyon are then considered more broadly to develop a generalized conceptual scheme for organic carbon transport and burial in submarine canyons.

2. Monterey Canyon

Monterey Canyon incises 30 km across the relatively flat ($<1.0^\circ$) continental shelf to near the shoreline at Moss Landing (Fig. 1). The canyon widens seaward from 800 m in the canyon head to 15 km at the shelf edge. The canyon has an average slope of 1.7° (e.g., Paull et al., 2005) along an axial channel with adjacent benches (morphologically defined as relatively flat areas above and adjacent to the axial channel; after Maier et al., 2012) along the canyon lower flanks.

The axial channel contains narrow and sharp turns in the upper canyon (here defined as 0–1000 m water depth), where it is incised through older canyon sediments

that record migration of the canyon position during the Pleistocene (after Maier et al., 2018). The lower canyon (here defined as 1000–2000 m water depths) contains broad axial channel bends incised into sedimentary and crystalline bedrock (e.g., Maier et al., 2018). The Monterey depositional system continues seaward from the lower canyon for >100 km, contributing to the Monterey Fan (e.g., Normark, 1970; Fildani and Normark, 2004).

Monterey Canyon is currently offset from rivers around Monterey Bay but intercepts sediment transported in littoral cells (e.g., Griggs and Hein, 1980; Inman and Jenkins, 1999; Farnsworth and Warrick, 2007). The canyon floor is dominated by coarse grained sand, gravel and larger clasts in the axial channel and finer-grained sediment with layers of silt and sand on the canyon benches and flanks (e.g., Paull et al., 2005, 2010a; Symons et al., 2017; Maier et al., 2019). Episodic sediment density flow events (commonly referred to as turbidity currents) move sand and gravel down the canyon axial channel up to multiple times a year, at velocities exceeding 4 m/s, and result in geomorphic change in the axial channel (e.g., Xu et al., 2008, 2014; Smith et al., 2005, 2007; Paull et al., 2010a, 2011, 2018; Symons et al., 2017; Maier et al., 2019). Between the episodic events, fine-grained sediment (median grain size silt) is transported through Monterey Canyon via internal tides and can be collected in sediment traps (Xu et al., 2014).

3. Methods

3.1. Approach

The focus of this study is the sediment and organic material collected in sediment traps during periods between episodic, powerful sediment density flow events along Monterey Canyon. Timing of sediment trap sub-samples along the CCE array is best constrained at the base of the sediment trap tubes, where sediment accumulated shortly after deployment, and thus, these samples are analyzed and compared in this study. We first discuss the sampling methodology, which allows interpretation of sediment trap samples in the context of internal tide sediment transport through Monterey Canyon, and as a basis to interpret down-canyon trends or the lack of trends. We then present analytical procedures, followed by a summary of portions of the CCE instrument dataset that most closely relate to, and thus, are the most relevant for interpretation of, sediment trap samples. We later compare these results to other submarine canyons, to create a general conceptual scheme for processes of organic carbon transport and deposition in submarine canyons.

3.2. Coordinated Canyon Experiment (CCE)

Three moorings in the upper canyon (MS1, MS2, MS3), and three in the lower canyon (MS4, MS5, MS7) (Fig. 1) were deployed during three consecutive six-month periods (I: October 2015 – April 2016; II: April – October 2016; III: October 2016 –

April 2017) (Paull et al., 2018). These moorings included oceanographic instruments and Anderson-type sediment traps at 10 to 300 meters above the seafloor (masf) (Paull et al., 2018; Lundsten, 2019; Maier et al., 2019). The CCE recorded 15 sediment density flow events moving down the canyon with maximum durations of 4–6 hours (Paull et al., 2018). The first sediment density flow event during deployments I, II, and III occurred on December 1, 2015, September 1, 2016, and November 24, 2016, respectively (Paull et al., 2018). We focus this study on sediment accumulated in traps before the first sediment density flow event in each deployment.

3.3. *Anderson-type sediment traps*

3.3.1. *Procedure for sample acquisition and processing*

Anderson-type sediment traps (Anderson, 1977; Rendigs et al., 2009) consist of an open top, baffled, fiberglass funnel (95–110 cm long, and ~25 cm diameter (0.05 m²) top opening) above a clear plastic liner tube (5–6 cm inner diameter) inside a PVC pipe (up to ~110 cm long) (after Maier et al., 2019) (Fig. 2). A dilute hypersaline solution of sodium azide (<5%) was added to most traps to deter bioturbation and preserve organic carbon content in the sample (e.g., Hedges et al., 1993). Intervalometers (after Rendigs et al., 2009) were used to insert up to 20 discs at pre-set intervals (typically every 8 days) into the liner tube to define sampling intervals. Liner tubes were stored upright in cold storage for ~1 month or more following recovery.

Sediment trap liner tubes were scanned with x-ray computed tomography (CT). In Deployment I, this was conducted using a GE LightSpeed Ultra instrument at the Stanford University Petroleum Research Institute (SUPRI-A) Enhanced Oil Recovery and Unconventional Resources laboratory facility, at 120 kV and 140 mA with 1.25 mm axial slices. In deployments II and III, this was conducted using a General Electric LightSpeed 16 CT scanner at the Lawrence Berkeley National Laboratory Rock Dynamic and Imaging Lab at 120 kV and 160 mA reconstructed to 0.625 mm axial slices.

Sediment from liner tubes were extruded in 1-cm intervals, split for grain size and other geochemical analyses, and stored in Whirlpak plastic bags (Maier et al., 2019). Deformation from sand loading into underlying fine-grained sediment occurred primarily in Deployment I samples (e.g., Fig. 3A). Sediment accumulation rates were estimated using averaged dry sediment density of fine-grained intervals of 0.95 g/cm³ and an average dry:wet ratio of 0.84. For traps with functioning intervalometers, apparent sediment accumulation rates were averaged from the 1-cm slices between discs. An average apparent sediment accumulation rate was calculated from the 1-cm slices accumulated over the entire deployment or before the first sediment density flow event (Table 1).

3.3.2. *Conceptual basis for sediment trap sample interpretation*

Geochemical analyses of samples from the bottom of the trap tubes represent approximately concurrent time periods across the CCE array from early in each deployment (i.e., April, October). Because the liner tubes on most traps filled before the end of each deployment and intervalometers were not available throughout the array, samples from the base of liner tubes have the greatest certainty for coincidence along the entire array. These samples represent ‘background’ sediment transport and intentionally exclude sediment density flow events (as defined in Paull et al., 2018 and interpreted from sediment traps in Maier et al., 2019) (Table 1).

Previous studies suggest that traps can provide a representative record of the composition of sediment and organic matter transported immediately over the trap, and results can be compared between traps of similar geometry (e.g., Gardner, 1980, 1989; Gardner et al., 1983b; Bruland et al., 1981; Buesseler et al., 2007; Liu et al., 2016). Anderson-type sediment traps were designed to measure flux of sediment settling vertically through the water column in quiescent, low-flow conditions (e.g., Anderson, 1977; Gardner, 1980, 1985). However, settling velocity of fine-grained sediment particles is orders of magnitude lower than even low horizontal current speeds (e.g., Gardner et al., 1997), and Anderson-type sediment traps function by fluid exchange of the water inside the trap with water from the passing current (e.g., Gardner, 1980, 1985). Baffles (Fig. 2B) reduce turbulence and grain size segregation (e.g., Anderson, 1977; Butman, 1986). Anderson (1977) noted that collection of fine-grained particles may be enhanced by high sediment concentration, allowing collection of measurable amounts of sediment over short time periods that can be sub-sampled and analyzed.

Although previous studies were mostly in lower flow velocity settings than Monterey Canyon, the underlying principles and methodology of the sediment traps from these earlier studies suggest that CCE traps likely provide reliable records of the sediment composition moving through Monterey Canyon. Gardner (1985) noted that trap tilt could result in fine-grained sediments $<63\ \mu\text{m}$ being over-collected relative to sediment $>63\ \mu\text{m}$, compared to rate of fall past a horizontal plane, but he found no statistically significant variations in organic matter content related to trap tilt. Gardner et al. (1983b) concluded that resuspension dominates sediment trap flux over trap tilt and current velocities.

Anderson-type sediment traps can be important tools for capturing representative samples of suspended sediment in high sediment flux areas. Similar trap designs have been used to interpret sediment transport in Gaoping Canyon (e.g., Huh et al., 2009b; Liu et al., 2012, 2016; Zheng et al., 2017), Hueneme and Mugu canyons (Xu et al., 2010). In this study, intervalometer discs and deployment dates constrain sediment that accumulated in the trap tubes prior to the first sediment density flow event during each CCE deployment. We acknowledge that the calculated in-trap sediment accumulation rates are ‘capture’ rates and may vary substantially from both the horizontal fluxes through the canyon and vertical accumulation rates on the seafloor (e.g., Xu et al., 2010;

Martín et al., 2011). Quantitative down-canyon comparisons herein assume that the Anderson-type sediment traps capture sediment in the same way throughout the CCE array, and thus, the apparent in-trap sediment accumulation rates and compositions provide useful down-canyon comparisons (e.g., Xu et al., 2010).

3.4. Laser particle grain size analyses

Grain size was measured on each 1-cm sub-sample from Deployment I, which showed similar grain size distributions within fine-grained intervals. Subsequently, grain size was measured more efficiently by analyzing only every fifth 1-cm sub-sample from deployments II and III. Laser particle grain size analyses used a Malvern II Mastersizer instrument measuring in quarter phi bins at the National Oceanography Centre Southampton (Maier et al., 2019). Grain-size samples were processed by (1) ~1 cm³ of each sample was added into measurement vials; (2) samples with grain sizes >2 mm were sieved to remove the fraction >2 mm; (3) 10% sodiumhexametaphosphate solution was added to make up to 20 ml solution in each sample pot; (4) samples were agitated on a mechanical shaker overnight (>12 hours); (5) the Malvern II autosampler was used to conduct the sampling; (6) random samples were selected and measured manually using the Mastersizer for comparison. Each sample was run three times and grain sizes averaged.

3.5. Radiocarbon analyses

Radiocarbon analysis focused on individual 1-cm sub-samples from near the base of liner tubes. Analyses were conducted at Beta Analytic Inc. (Florida, USA) using standard accelerator mass spectrometry (AMS) procedure. Samples were pretreated with repeated liquid acid (HCl) washes until carbonate material was removed, according to Beta Analytic Inc. acid washes pre-treatment procedure. The remaining organic carbon sample was converted to graphite for AMS analysis. Results are reported as $\delta^{13}\text{C}$ -corrected percent modern carbon (pMC) after Stuiver and Polach (1977).

3.6. Organic carbon analyses

Organic carbon stable isotopes $\delta^{13}\text{C}$ and $\delta^{15}\text{N}$ have been used to distinguish terrestrial and marine sources (e.g., Peters et al., 1978; Paull et al., 2006; Prouty et al., 2017). As a simplified general distinction herein, marine organic carbon is considered as having $\delta^{13}\text{C}$ values between -22 and -20 per mil (PDB) and $\delta^{15}\text{N}$ values >+7 per mil (air) (e.g., Peters et al., 1978; Cifuentes et al., 1988; Paull et al., 2006). Likewise, terrestrial organic carbon is considered as having $\delta^{13}\text{C}$ values between -25 and -23 per mil (PDB) and $\delta^{15}\text{N}$ values <+3 per mil (air) (e.g., Peters et al., 1978; Cifuentes et al., 1988; Paull et al., 2006). Organic carbon stable isotope and total organic carbon values, analyzed as in this study, are available from two samples of the nearby Salinas River ($\delta^{13}\text{C}$: -26.5 per mil; TOC: 0.18) and Pajaro River ($\delta^{13}\text{C}$: -23.7 per mil; TOC: 0.37) (Paull et al., 2006).

Stable isotopes from organic material ($\delta^{13}\text{C}$, $\delta^{15}\text{N}$) and total organic carbon content were measured from two fine-grained 1-cm sub-samples per trap from the base of the tube and from 5–10 cm above. Analyses were conducted at the Stanford Stable Isotope Laboratory at Stanford University, California, using a Carlo Erba NA1500 Series II elemental analyzer and a Finnigan MAT 252 isotope ratio mass spectrometer. An initial set of 23.9–24.1 microgram samples were acidified with liquid sulfurous acid (for at least 24 hours at room temperature until no reactions were apparent) to remove carbonate and analyzed for total organic carbon content, $\delta^{13}\text{C}$, and C/N atomic ratio using L-glutamic acid USGS-40 standard reference material 8573 and acetamide conditioner. A secondary set were analyzed without acidification for $\delta^{15}\text{N}$.

3.7. ^{210}Pb analyses

Excess ^{210}Pb activity ($x\text{s}^{210}\text{Pb}$; $t_{1/2} = 22.23$ years) is widely used as a chronometer in recent (<200 years) sediments (e.g., Swarzenski, 2014 and references therein). Supported, time-independent ^{210}Pb is present in recent sediments from decay of ^{226}Ra as part of the ^{238}U decay chain (e.g., Kirchner, 2011). Excess, time-variable ^{210}Pb is produced in the atmosphere through decay of ^{222}Rn , transported via wet and dry deposition to the Earth surface, and adsorbed (i.e., scavenged) by fine-grained particulate matter in the water column (e.g., Xu et al., 2010; Kirchner, 2011; Swarzenski, 2014).

Excess ^{210}Pb activity ($x\text{s}^{210}\text{Pb}$) was analyzed from traps at the shallowest (MS1), middle (MS3), and deepest (MS7) part of the CCE mooring array. Three consecutive 1-cm sub-samples of fine-grained sediments from near the base of trap tubes were combined, oven-dried, finely-ground, and homogenized. Approximately 6–10 g of sample was analyzed with gamma-spectroscopy in small-volume HPGe well detectors at the U.S. Geological Survey in Santa Cruz, California, following methods described in Swarzenski et al. (2006) and Xu et al. (2010). Excess ^{210}Pb activity was calculated as the difference between total ^{210}Pb and supported ^{210}Pb from decay of ^{226}Ra ($x\text{s}^{210}\text{Pb} = \text{total}^{210}\text{Pb} - ^{226}\text{Ra}$) (e.g., Xu et al., 2010; Swarzenski, 2014).

3.8. Oceanographic instrumentation

Portions of the CCE instrument dataset (Paull et al., 2018) that are immediately relevant to the sediment trap samples are summarized in this study (see also Ferreira et al., 2019). Downward-looking 300 kHz acoustic Doppler current profilers (ADCPs) at 65 m (e.g., Fig. 2A) measured velocity in 7-ping ensembles every 30 seconds, and plots presented here from individual bins of ADCP data show 2-minute averages of the 30-second ensembles. Statistics for current speeds along the canyon are derived from ADCP data using the closest reliable 1-meter bin to the seafloor at each mooring for deployments II and III because MS1 was ripped off its anchor during Deployment I, resulting in a complete dataset throughout the entire array only in deployments II and III (see Paull et al., 2018). Turbidity sensors measured every minute. Transmissometer beam

attenuation was used to estimate concentration of fine-grained sediment captured in traps, following Xu et al. (2002a), and converted to along-canyon flux using ADCP velocity at 10 masf. To relate transmissometer-derived suspended sediment concentrations with sediment trap samples, sediment and organic carbon flux are estimated in the upper canyon for the first 32 internal tidal cycles (e.g., Wang et al., 2009; Xu and Noble, 2009) from Deployment III, when the same type of transmissometers were deployed on MS1, MS2, and MS3 at approximately 10 masf. A directional wave gauge, deployed on the continental shelf outside of Monterey Canyon (WHS in Fig. 1), acquired 1 Hz measurements for 17 minutes every 2 hours.

3.9. Sediment cores used for comparison of organic carbon transport and deposition

We compare new sediment trap analyses in this study to previous organic carbon analyses by Paull et al. (2006) of fine-grained sediment in and around Monterey Canyon. These include sediment core samples collected between 1999 and 2002 along Monterey Canyon axial channel, adjacent benches, and flanks in 107–1169 m water depths, as well as grab samples and suspended sediment samples from surrounding nearshore areas and rivers. Paull et al. (2006) selected clay-rich sediment core sub-samples (from the seafloor to >5 m depth in the cores) for organic carbon analyses (including $\delta^{13}\text{C}$, $\delta^{15}\text{N}$, $\delta^{14}\text{C}$, total organic carbon) from clay clasts within the canyon axial channel and accumulated fine-grained sediments draping the axial channel, benches and flanks up to 129 m above. Notably, the Paull et al. (2006) organic carbon stable isotope analyses were conducted in the same manner and in the same laboratory as trap samples in this study.

4. Results

4.1. Sediment traps and grain size

A total of 25 Anderson-type sediment traps were successfully recovered during the CCE (Table 1). Nine of the traps contained intervalometers that released discs throughout the liner tubes (Table 1; Fig. 3), showing that liners filled and began to overflow before the deployment ended. The in-trap sediment accumulation rate measured with intervalometers in the upper canyon traps (MS1, MS2, MS3) was over twice as rapid compared to the lower canyon traps (MS5). In-trap sediment accumulation rates along the entire array are comparably high (up to hundreds of $\text{g}/\text{m}^2/\text{day}$) between deployments and estimation methods, and generally decrease down-canyon (Table 1).

CT scans and grain size analyses show that traps filled primarily with fine-grained sediment which contain subtle <1-cm-thick layers (Fig. 3). Grain size distributions averaged from measurements throughout the fine-grained units are unimodal with median grain sizes between 13–18 μ , and slightly coarser (median grain size 22–27 μ) at MS1 (Fig. 4; Supplementary Table 1). Fine- to coarse-grained sand intervals correspond to the timing of sediment density flow events recorded by ADCPs (Paull et al., 2018) and are concentrated in mid- to upper portions of the tubes (e.g., Fig. 3A, C). Additional sandy

(d0.9 up to 200 μ) units are present at MS1 (asterisks in Fig. 3A, C).

4.2. Radiocarbon analyses

Percent modern carbon from radiocarbon analyses of 23 individual 1-cm samples ranges from 87.2 ± 0.3 to 67.5 ± 0.3 , which equates to conventional radiocarbon ‘ages’ of $1100 - 3160 \pm 30$ years before present (without reservoir corrections; Stuiver and Polach, 1977) (Fig. 5; Supplementary Table 2). Analyses are from traps at ~ 10 –300 masf, but most of the analyzed samples were from traps at ~ 10 masf. No systematic changes are apparent between the three deployments or down-canyon. Lowest pMC values occur with depleted $\delta^{13}\text{C}$ values in deployments II and III, suggesting that, in some time periods, younger carbon may be preferentially provided by marine sources.

4.3. Organic carbon content and stable isotope analyses

Total organic carbon content (TOC) and stable isotopes were analyzed from 50 individual 1-cm-extruded trap samples (Figs. 6, 7; Supplementary Table 3). TOC increases down-canyon, from 1.2 to 2.9 weight percent (Fig. 6A). Nitrogen isotopes ($\delta^{15}\text{N}$) range from 5.8 to 7.4 per mil (Fig. 7B), and nitrogen content ranges from 0.2 to 0.4 weight percent. $\delta^{13}\text{C}$ ranges from -22.2 to -24.4 per mil (PDB), but only four samples resulted in $\delta^{13}\text{C} < -23.0$ per mil (Fig. 7; Supplementary Table 3). Carbon-nitrogen (C:N) atomic ratios range from 7.9 to 9.4 (Supplementary Table 3). Increasing carbon and nitrogen stable isotopes show significant correlations ($p < 0.05$) only for the Deployment II (Fig. 7B), and carbon isotopes are enriched down-canyon only in one set of samples from the Deployment II (Fig. 7A).

4.4. ^{210}Pb analyses

Excess ^{210}Pb ($x_s^{210}\text{Pb}$; dpm/g) activities consistently increase down-canyon (Fig. 8A; Supplementary Table 4). $x_s^{210}\text{Pb}$ activities are over three times greater at MS7 ($56.2 - 73.9 \pm 1.1 - 1.4$ dpm/g) than at MS1 ($13.6 - 18.3 \pm 0.6 - 0.7$ dpm/g). The MS7 $x_s^{210}\text{Pb}$ activity in the trap at 300 masf is greater than in the trap at 10 masf on the same mooring. Measured $x_s^{210}\text{Pb}$ activities increase with increasing weight percent TOC measured from the same trap (Fig. 8C). Small amounts of ^{137}Cs are measured in all samples (mean 0.13 dpm/g, standard deviation 0.05 dpm/g), but no trends are apparent between traps or deployments (Supplementary Table 4).

4.5. Instrument measurements

Oscillations in along-canyon velocity and turbidity occur throughout the mooring array, related to semi-diurnal and diurnal internal tidal flows within Monterey Canyon (e.g., Wang et al., 2009; Xu and Noble, 2009). Along-canyon velocities, measured by the ADCPs, alternate orientation up- and down-canyon sub-daily, and occur with fluctuations in turbidity (e.g., Fig. 9; Ferreira et al., 2019). Notably, up-canyon velocities at 10 masf

reach 1 m/s at the shallowest mooring (MS1; 287 meters water depth) (Fig. 9A). Mean current speeds range from 12.4 to 19.8 cm/s at a single mooring and deployment (Table 2). Many up-canyon and down-canyon peaks in ADCP-measured velocity at 10 or 65 masf on MS1 coincide with peaks in turbidity measured by a sensor at 35 masf, while other turbidity peaks coincide with the switching orientation of the internal tide at MS1 (Fig. 9A, B).

Suspended sediment fluxes are estimated herein for a rough comparison to the Anderson-type sediment traps. Suspended sediment concentrations, estimated from transmissometers at 10 masf, were ≤ 0.03 g/L for MS1 and < 0.02 g/L for MS2 and MS3 during the first 16 days of Deployment III (Fig. 10), when the same type of transmissometers were deployed on MS1, MS2, and MS3 at approximately 10 masf. Suspended sediment flux varied between $0.02 \text{ kg/m}^2/\text{s}$ down-canyon and $0.01 \text{ kg/m}^2/\text{s}$ up-canyon. Most sediment fluxes were $< 0.005 \text{ kg/m}^2/\text{s}$. Cumulative suspended sediment flux through a square meter vertical cross-section of the canyon at the mooring sites during the first 16 days (32 tidal cycles) of Deployment III were $1.25 \cdot 10^6 \text{ kg}$ down-canyon at MS1, $1.60 \cdot 10^5 \text{ kg}$ up-canyon at MS2, and $2.36 \cdot 10^5 \text{ kg}$ down-canyon at MS3.

The wave height record from the continental shelf south of Monterey Canyon (WHS in Fig. 1) contains variation on the order of meters within days (Paull et al., 2018). The top tenth percentile of wave heights (H10) can exceed 3.0 meters (Fig. 11). Mean direction and peak period direction during these spikes in wave height are oriented towards the northeast and southeast.

5. Discussion

5.1. How are fine-grained sediment and organic carbon transported in a submarine canyon between sediment density flow events?

Monterey Canyon experiences persistent, dynamic sediment and organic carbon transport that is concentrated near the seafloor along the canyon's axial channel. This includes sub-daily variations in velocity and turbidity (e.g., Fig. 9) that are interpreted to be primarily the result of semi-diurnal and diurnal internal tides within Monterey Canyon (e.g., Petruncio et al., 1998; Xu et al., 2002b; Xu and Noble, 2009). Internal tidal flow velocities documented in the CCE ADCP measurements exceed previous velocity measurements and estimations in Monterey Canyon (Petruncio et al., 1998; Xu et al., 2002b; Xu and Noble, 2009; Jingling et al., 2015). Unlike the adjacent continental shelf (Rosenberger et al., 2016), internal tides appear to be an important mechanism in sediment transporting sediment and organic carbon within Monterey Canyon, dominating between sediment density flow events. Internal tide sediment and organic matter transport also may be important for canyon ecosystems, providing food to filter-feeding organisms and possibly influencing distributions of canyon biomass (e.g., Shea and Broenkow, 1982; Amaro et al., 2015, 2016; Prouty et al., 2017).

Sediment flux estimates (e.g., Fig. 10) provide a broad, first-order comparison for

flux near the canyon floor during background, internal-tide-dominated conditions. We note that these estimates only included 16 days of data (corresponding to the sediment trap samples analyzed herein) and suggest a convergence of flux in the upper canyon (net down-canyon at MS1 and MS3 with net up-canyon at MS2), which is clearly not representative of persistent, long-term conditions throughout the water column in these locations. This apparent discrepancy may result from some cross-canyon (orthogonal to along-canyon flows) shear in the flow (leading to the net up-canyon flux observed at MS2), or there may be a return flow farther up in the water column that is not captured in the CCE near-seafloor dataset.

The lateral organic carbon flux can be estimated by combining the TOC (weight %) analyses with suspended sediment flux (Fig. 10). Organic carbon flux for the first 16 days of Deployment III at 10 m above the seafloor was net down-canyon $1.8 \cdot 10^4 \text{ kg/m}^2$ at MS1 and $4.7 \cdot 10^3 \text{ kg/m}^2$ at MS3. Because MS2 sediment traps were ripped from the mooring during Deployment III, we use an average of TOC analyses from deployments I and II to estimate organic carbon flux for the first 16 days in Deployment III at 10 m above the seafloor of $2.56 \cdot 10^3 \text{ kg/m}^2$ up-canyon at MS2. As with sediment flux, these estimates may not be representative of longer timescales or across the entire canyon cross-section.

We interpret that internal tide sediment transport and resuspension result in the fine-scale layering and high accumulation rates of fine-grained sediments in the near-seafloor (primarily 10 masf) sediment traps (Table 1; Fig. 3). The coarser (fine sand to silt), thin (<1 cm) layers (Fig. 3) appear to record variations in sediment transported by internal tides that intensify up-canyon. This interpretation is similar to where Xu et al. (2010) noted strong internal tidal currents suspending sandy sediment (46% sand) that was collected in sediment traps 60 masf in Hueneme and Mugu submarine canyons, offshore southern California. Similarly, the internal tide in Gaoping Canyon increased the coarse fraction present in Anderson-type sediment traps (Liu et al., 2016). A bottom nepheloid layer composed of resuspended sediment (e.g., Drake and Gorsline, 1973; Xu et al., 2002b) may be repeatedly moved past the Monterey Canyon moorings by internal tides, resulting in high apparent sediment accumulation rates in sediment traps (Table 1). Increases in internal tide velocities may amplify coarse sediment transport and total sediment accumulation in traps, but the complex association of velocity, turbidity, and timing of trap accumulation cannot be further distinguished from intervalometer discs alone in this study (e.g., Fig. 9A, B).

The fine-scale layering in the sediment trap on MS1 is augmented by thicker (≤ 5 cm), sandier layers that did not coincide with the timing of sediment density flow events (after Paull et al., 2018) or with strong internal tide events (Fig. 11). We suggest that these thicker, sandier layers may accumulate in association with increased wave height on the adjacent shelf oriented towards the southeast or northeast during deployments I and III (Fig. 11). Sediment resuspension and transport on the shelf adjacent to the canyon

could have moved sediment over the rim of the canyon to the north and (or) south of MS1 (Fig. 1). Similar shelf re-working and resuspension by storms was interpreted from traps in Hueneme and Mugu canyons, offshore southern California, where these two canyons incise close to the shoreline and remain in close proximity to the shelf (Inman et al., 1976; Xu et al., 2010).

5.2. *How is organic carbon fractionated and (or) mixed along the canyon?*

We consider mixing and along-canyon trends during periods between episodic sediment density flow events (i.e., only during background conditions). The observed down-canyon increase in the concentration of organic carbon (measured weight percent TOC; Fig. 6A) appears to reflect higher input of clastic sediment nearer the canyon head. Overall sediment accumulation rates in traps decrease down-canyon (Table 1; Fig. 3), such that a 1-cm sub-sample from a lower canyon trap at 10 masf represents a longer timeframe than a 1-cm sub-sample from an upper canyon trap at 10 masf. Normalizing TOC measurements for in-trap accumulation rates results in a down-canyon decrease in the rate of organic carbon delivery (g/day TOC; Fig. 6B). Clastic sediment may have settled more rapidly than organic matter with down-canyon decreases in internal tide velocities. This could have resulted in an increase in the fraction of organic matter relative to clastic sediment (weight percent TOC), despite a decrease in organic carbon flux down-canyon (g/day TOC).

Lack of consistent down-canyon trends in pMC (Fig. 5A) and organic carbon stable isotopes (Fig. 7) suggests effective mixing of organic carbon composition in the water column, likely by internal tides. Sediment and organic carbon moving through the canyon represent a mixture of sources, including marine, terrestrial, and resuspended canyon deposits. Organic carbon isotopic signatures measured from traps likely represent a mixture of terrestrial and marine sources (Fig. 7), but may also reflect variability in marine sources noted in surface waters above the Monterey Bay continental shelf adjacent to the canyon (Rau et al., 2001). Terrestrial to mixed terrestrial-marine endmember $\delta^{13}\text{C}$ signatures (-24.4 to -22.2 per mil) occur throughout the Monterey Canyon sediment trap array (Fig. 7), and C:N ratios (7.9–9.4) are consistently higher than marine organic material (6.7; Redfield, 1934), suggesting a likely input of terrestrial organic material along the canyon near-seafloor from adjacent rivers and (or) resuspension. Secondary mobilization of older canyon deposits along the upper canyon (e.g., Paull et al., 2006, 2010a, b; Maier et al., 2018) through internal tide resuspension and (or) sediment density flow events may contribute to isotopic signatures and TOC measured from sediment trap samples. However, the average pMC of trap samples (Fig. 5; Supplementary Table 2) is similar to that of water column samples from Moss Landing Harbor and immediately offshore (Paull et al., 2006). In addition, water column productivity and resuspension of nepheloid layer material from the adjacent continental shelf or canyon likely contribute to TOC, pMC, and organic carbon isotopic signatures in

Monterey Canyon during non-event periods.

5.3. How are transported organic carbon and fine-grained sediment preserved in canyon deposits?

5.3.1. Organic carbon burial

Available organic carbon analyses of fine-grained sediments collected in cores from deposits in Monterey Canyon prior to the CCE (Paull et al., 2006) warrant comparison to organic carbon transported through the canyon that is captured in CCE sediment traps. Trap samples, reflecting sediment that moves through the canyon via internal tides, have organic carbon with enriched $\delta^{13}\text{C}$ and $\delta^{15}\text{N}$ (likely more marine signature) compared to organic carbon preserved in sediment cores (Fig. 12A, B). Core samples from Paull et al. (2006) lack the down-canyon trends in TOC found in traps (Fig. 12C). The two sample sets are lithologically similar fine-grained sediment, although the same type of grain size analyses are not available for canyon floor deposits that were analyzed for organic carbon, and thus, grain size effects are possible. Notably, the two sample sets are from different time periods and locations in the canyon, yet the Paull et al. (2006) core analyses are the best sample set available for comparison with trap analyses from this study.

Comparison of these two available sample sets suggests that seafloor deposits may substantially underestimate the composition and supply of organic carbon in the suspended sediment moving within the canyon. For example, first-order estimates of burial efficiency can be made by dividing TOC results from core samples in Paull et al. (2006) ($0.5 \pm 0.4\%$; average and single standard deviation) by TOC results in the nearby sediment trap samples ($1.9 \pm 0.3\%$) (e.g., Fig. 12C). Both sample sets are analyzed from fine-grained material, but Paull et al. (2006) cores are dominantly from higher above the axial channel than traps at 10 masf. The ratio of TOC in background sediment in traps located 10 m above the axial channel floor and fine-grained deposits in cores results in organic carbon specific burial efficiency estimate of ~26%.

Sediment transport processes will influence organic carbon burial efficiency. Our analyses in Monterey Canyon exclude (sand-dominated) turbidity current units in sediment trap samples (Maier et al., 2019). Sandy-deposits that dominate the canyon floor may have lower organic carbon contents, as organic carbon is preferentially associated with fine-grained deposits (e.g., Masson et al., 2010). Paull et al. (2006) do not distinguish between organic carbon contents of fine-grained background settling and fine-grained turbidity current deposits, which likely are both contained in fine-grained sediment accumulating along the canyon floor and lower flanks (e.g., Paull et al., 2010a; Symons et al., 2017). It remains unclear whether mud-rich seafloor deposits from turbidity currents have higher or lower organic carbon contents than deposits from background sediment transport analyzed from sediment traps; and thus, it is not possible to determine exactly how inclusion of flow deposits in seafloor cores affects organic

carbon burial efficiency estimates. In this study, we can provide only specific burial efficiency estimates, meaning that they incorporate only background sediment transport. If turbidity current deposits have relatively low organic carbon contents compared with background sediment transport, then incorporating turbidity currents would increase our burial efficiency estimates. Conversely, burial efficiency estimates might decrease if sediment and organic matter in traps are derived largely from internal tide resuspension and contain a mixture of new and resuspended seafloor organic carbon (e.g., Masson et al., 2010).

As noted by Masson et al. (2010), differences in sedimentation accumulation rates should be considered in estimates of organic carbon burial efficiency because burial efficiency calculations should compare total amounts of sediments deposited over a unit of time, rather than organic carbon abundance per unit volume of sediment. For example, corrections based on differences in trap and core sediment accumulation rates decreased Nazaré Canyon organic carbon burial efficiency calculations from ~80% to ~30% (Masson et al., 2010). Our trap samples and Paull et al. (2006) core samples are not from the same time period, but both can be approximately converted into accumulation over unit time, as a first-order comparison. Accumulation rates of organic carbon in traps are 0.2 ± 0.1 g/day, estimated using TOC (weight percent) and averaged density and water content (Fig. 6B; Supplementary Table 3). Sedimentation rates of Paull et al. (2006) core samples are estimated over a longer time-scale where pollen data suggests >5 m sediment accumulation in historic times (i.e., 5 m in 200 years; ~0.007 cm/day), which suggests sediment accumulation on the seafloor that is >140 times slower than trap accumulation. If we estimate sediment density in the core samples as similar to the trap samples and use Paull et al. (2006) reported TOC values (weight percent) with a core diameter of 7.8 cm (e.g., Paull et al., 2010a), then the core sediments accumulated organic carbon at ~0.002 g/day. Thus, if sediment accumulation rates are incorporated, then estimates of organic carbon specific burial efficiency in upper Monterey Canyon decrease by orders of magnitude from ~26% to ~0.1%. Despite the large CCE dataset that facilitates these first-order estimates, additional investigation is needed to better constrain organic carbon burial efficiency calculations in this and other submarine canyons.

A likely contributor to organic carbon specific burial efficiency and isotopic signatures preserved through time is post-depositional alteration. Oxidation, bioturbation and metabolism of organic matter on the seafloor by grazing and infaunal organisms (e.g., Lehmann et al., 2002; Baudin et al., 2017; Symons et al., 2017), and local ecosystem variability (e.g., Martiny et al., 2013) will influence the organic carbon preserved in sediment deposits. For example, preferential consumption of organic carbon with greater pMC and enriched $\delta^{13}\text{C}$, would deplete the measured organic carbon $\delta^{13}\text{C}$ and enhance the more terrestrial signature observed in seafloor deposits compared with sediment trap samples (e.g., Fig. 12). Likewise, degradation of organic material on the canyon floor may deplete $\delta^{15}\text{N}$ in seafloor deposits relative to trap samples (e.g.,

Lehmann et al., 2002). Lesser organic matter degradation and consumption in sodium azide-treated trap samples (e.g., Gardner et al., 1983a) preserves a snapshot of organic carbon available to organisms in the canyon. Additionally, use of hypersaline brine in sediment traps might have resulted in under-collection of low-density organic matter (e.g., Fawcett et al., 2018), which would imply under-measurement of TOC in this study and result in even lower specific burial efficiency estimates.

Previous studies have also estimated organic carbon burial efficiency by comparing river sediment to submarine canyon deposits. For example, a study of the Bengal Fan system (Galy et al., 2007) compared similar organic carbon abundance in river sediment and deep-sea cores, suggesting much more efficient organic carbon burial than estimated in this study for Monterey Canyon. It is also instructive to compare organic carbon content supplied by rivers around Monterey Bay to those in Monterey Canyon traps and deposits. We note that, at present, sediment is dominantly supplied to Monterey Bay by longshore drift, and ultimately the rivers supply sediment into the coastal systems. TOC (weight percent) in the Salinas and Pajaro river beds (<0.5%; Paull et al., 2006) is much lower than in sediment traps (1.2–2.9%), but comparable to seafloor core samples (0.5 %; Paull et al., 2006) (Fig. 12C). This suggests a possible higher specific burial efficiency when comparing only river and canyon floor samples.

5.3.2. Patterns in fine-grained sediment from excess ^{210}Pb activities

Analyses of xs^{210}Pb activities from Monterey Canyon sediment traps provide a geochemical tool to evaluate fine-grained sediment transport and deposition in conjunction with organic carbon analyses. Increasing water depths along the CCE sediment trap array increase the amount of time that particles falling vertically through the water column had to adsorb xs^{210}Pb (e.g., Lewis et al., 2002; Martín et al., 2006; Alexander and Venherm, 2003); however, adsorption from vertically settling particles does not account for the high measured xs^{210}Pb activities in Monterey Canyon near-seafloor sediment traps. For example, the atmospheric ^{210}Pb deposition rate of 4.1 dpm/m²/day for central California (Fuller and Hammond, 1983) and maximum xs^{210}Pb scavenging of 9.4 dpm/m²/day from sediment settling vertically through 800 m water depth would result in measured xs^{210}Pb activities of ~14 dpm/m²/day (after Alexander and Venherm, 2003). This maximum amount of xs^{210}Pb produced from vertical settling is orders of magnitude less than the measured xs^{210}Pb activities from MS3. If adsorption via vertical settling controlled xs^{210}Pb activities in Monterey Canyon sediment traps, then xs^{210}Pb activity (dpm/g) in a trap at 300 masf would not have been greater than a contemporaneous measurement from 290 meters closer to the seafloor on the same mooring (Fig. 8A). Sediment transported laterally near the seafloor via internal tides can adsorb significantly more xs^{210}Pb than would have been possible from vertical settling alone (e.g., Krishnaswami et al., 1975; Smoak et al., 2000; Alexander and Venherm, 2003).

The observed down-canyon increase in $x_s^{210}\text{Pb}$ activities (dpm/g) (Fig. 8A) is primarily a result of down-canyon decrease in sediment accumulation rate. This inverse relationship has been widely noted in other submarine canyons (e.g., Hung and Chung, 1998; Palanques et al., 2005; Martín et al., 2006, 2011; de Stigter et al., 2007; Huh et al., 2009b; Xu et al., 2010; Prouty et al., 2017). As in-trap accumulation rates decrease, a gram of analyzed sub-sample represents a longer time interval, resulting in higher $x_s^{210}\text{Pb}$ activities (dpm/g).

Weight percent TOC also increases down-canyon and may add to trends in $x_s^{210}\text{Pb}$ activities (dpm/g) (Fig. 8C). Yang et al. (2015) suggested that higher organic carbon content could increase ^{210}Pb adsorption onto inorganic nanoparticles. However, the $x_s^{210}\text{Pb}$ (dpm/g) trend is not apparent when $x_s^{210}\text{Pb}$ activities are normalized for sediment accumulation rate (dpm/day) (Fig. 8B), suggesting no systematic variation of scavenging or $x_s^{210}\text{Pb}$ availability related to organic carbon delivery.

The possible influence of grain size on the down-canyon trend in $x_s^{210}\text{Pb}$ activities (dpm/g) (e.g., Kirchner, 2011) was also considered. Although MS1 is slightly coarser, background grain size is similar throughout the remainder of the array (Fig. 4). This suggests that grain size has little contribution to the down-canyon increase in $x_s^{210}\text{Pb}$ activities (dpm/g).

Xu et al. (2010) noted that $x_s^{210}\text{Pb}$ activities in sediment transported through Hueneme and Mugu canyons, offshore southern California, was diluted by low $x_s^{210}\text{Pb}$ activities in laterally transported sediments resuspended from the shelf or canyon walls during storms. Down-canyon trends in $x_s^{210}\text{Pb}$ activities (dpm/g) in this study are likely related to sediment transported and resuspended by internal tides, wherein the upper canyon sediment both spend less time in the water column adsorbing ^{210}Pb than lower canyon samples and may be resuspended from relatively ^{210}Pb -poor upper canyon deposits.

Measured $x_s^{210}\text{Pb}$ activities of sediment moving through the canyon are fundamentally different than, but have implications for, ^{210}Pb analyses on sediment sampled from seafloor deposits. In sediment cores, the ^{210}Pb profile is used as a chronometer and measure of deposition rates (e.g., Lewis et al., 2002; Zúñiga et al., 2009). Notably, the down-canyon increase in $x_s^{210}\text{Pb}$ activities (dpm/g) from traps is apparent in the $x_s^{210}\text{Pb}$ activities (dpm/g) measured from the top centimeter of seafloor sediments adjacent to the CCE sediment traps (Fig. 12D). Previous studies of organic carbon signatures (Fig. 12A–C; Paull et al., 2006), and canyon facies (e.g., Paull et al., 2010a; Symons et al., 2017) suggest that fine-grained bench deposits may be predominantly sediment density flow deposits, but $x_s^{210}\text{Pb}$ activities of fine-grained sediment in canyon bench deposits appear to be recording an aspect of along-canyon trends in the water column, possibly related to internal tide transport and resuspension of fine-grained sediment.

5.4. *Implications for submarine canyon studies*

5.4.1. *Submarine canyon deposits*

Sediment traps provide direct samples of sediment moving through the water column but do not necessarily reflect the lithology or geochemistry of sediment deposited and preserved on the seafloor in submarine canyons. Despite the importance of internal tides in Monterey Canyon, seafloor samples may not reflect sediment or organic carbon transported via internal tides; instead deposits along and near the canyon axial channel appear to be dominated by episodic and powerful sediment density flow events (e.g., Paull et al., 2005, 2010a; Maier et al., 2019). In particular, organic carbon analyses of fine-grained seafloor deposits are distinctly different than nearby traps (Fig. 12). Sediment sampled from seafloor deposits show little clear record of internal tide signatures, background sediment transport, and organic carbon available to deep-sea communities in the canyon, except in $xs^{210}\text{Pb}$ activity (dpm/g) down-canyon trends. This is critical to address in more detail in the future because much of our knowledge of submarine canyons through geologic time is derived from their remaining deposits (e.g., Talling et al., 2015; Covault et al., 2016). Studies in other submarine canyons and deep-water settings have interpreted internal tide processes from deposits without the benefit of direct measurements and sampling achieved in this study with sediment traps (e.g., Zhenzhong and Eriksson, 1991; Kudrass et al., 1998; Shanmugam, 2003; He et al., 2011; Pomar et al., 2012), and others have noted that accumulation of sediment in upper canyon traps exceeds contemporaneous seafloor deposition (e.g., de Stigter et al., 2007). It appears that internal tides are a significant, consistent process moving sediment through Monterey and other submarine canyons that may not be adequately reflected in seafloor deposits.

5.4.2. *Generalized scheme and comparisons*

Below, we briefly compare Monterey Canyon results with other submarine canyons where focused study has provided estimates of accumulation in sediment traps, internal tide velocities, and (or) organic carbon delivery and burial efficiency. We use Nazaré Canyon, Gaoping (Kaoping) Canyon, and Whittard Canyon to discuss similarities and variability in internal tides and organic carbon in submarine canyon environments.

5.4.2.1. Nazaré Canyon: Like Monterey Canyon, Nazaré Canyon, offshore the Western Iberian Margin, is incised to near the shoreline and contains sandy crescentic-shaped bedforms along the canyon axis (e.g., Arzola et al., 2008). Internal tidal flows decrease down Nazaré Canyon and have been measured up to 80 cm/s along with sediment trap apparent accumulation rates (mean 65 g/m²/day; maximum 265 g/m²/day) on the order of those in this study (de Stigter et al., 2007; Martín et al., 2011). Despite these similarities between Nazaré and Monterey canyons, organic carbon contents in sediment traps from upper Monterey Canyon generally are lower than in Nazaré Canyon, although some Nazaré Canyon sites are in deeper water depths and at greater distances offshore than upper Monterey Canyon (Epping et al., 2002; Masson et al., 2010).

Likewise, Masson et al. (2010) organic carbon burial efficiency estimates from Nazaré Canyon are much higher than the specific burial efficiency estimates from Monterey Canyon in this study, including ~80% compared with ~26% by direct core and trap comparison, and ~30% compared with ~0.1% when accounting for sediment accumulation rates. Higher organic carbon content in cores from Nazaré Canyon compared with Monterey Canyon may be related to the overall muddier sediments in Nazaré Canyon (e.g., Arzola et al., 2008; Pusceddu et al., 2010), even compared with fine-grained sediment accumulation along Monterey Canyon benches (e.g., Paull et al., 2006, 2010a; Symons et al., 2017). Organic carbon delivery to Nazaré Canyon decreases down-canyon, as in Monterey Canyon, and has been demonstrated to impact fauna and food webs within the submarine canyon environment (van Oevelen et al., 2011).

5.4.2.2. Gaoping (Kaoping) Canyon: Gaoping (Kaoping) Canyon, offshore Taiwan, can be compared with Monterey Canyon particularly because similar Anderson-type sediment traps have been deployed in studies of both canyons (e.g., Huh et al., 2009b; Liu et al., 2012, 2016; Zheng et al., 2017). Like Monterey and Nazaré canyons, Gaoping (Kaoping) Canyon heads near the shoreline, and sedimentation rates are high (e.g., Huh et al., 2009a). As in Monterey Canyon, internal tidal flows in Gaoping (Kaoping) Canyon reach >1 m/s near the seafloor, facilitate a bottom nepheloid layer, impact benthic communities, and transport fine-grained sediment into traps deployed in the canyon (e.g., Lee et al., 2009; Liu et al., 2010, 2013, 2016; Liao et al., 2017). Apparent sediment accumulation rate estimates for traps are within similar ranges in Gaoping (Kaoping) and Monterey canyons (Liu et al., 2016). However, the two canyons differ in organic carbon content (overall lower in Gaoping (Kaoping) than in Monterey, particularly during internal-tide-dominated intervals) and $\delta^{13}\text{C}$ (more depleted in Gaoping (Kaoping) compared with Monterey), likely owing to the higher terrestrial input to Gaoping (Kaoping) Canyon from hyperpycnal and hypopycnal flows, frequent typhoons, and abundant sediment run-off (e.g., Kao et al., 2014; Liu et al., 2016; Zheng et al., 2017). Accordingly, organic carbon burial efficiency may be higher in Gaoping (Kaoping) Canyon than specific estimates from Monterey Canyon, owing to the muddier sediment and rapid transport and deposition of river sediment into Gaoping (Kaoping) Canyon head (e.g., Huh et al., 2009a; Liu et al., 2009, 2013; Liao et al., 2017).

5.4.2.3. Whittard Canyon: Powerful sediment density flows occur much less frequently in Whittard Canyon because the Whittard Canyon head is >300 km from the shoreline and thus, terrestrial sediment sources (Amaro et al., 2016). Whittard Canyon nevertheless remains a dynamic environment for benthic ecosystems, sediment transport, and organic matter transport and mixing, owing to internal tide velocities >40 cm/s that intensify towards the seafloor (e.g., Amaro et al., 2016; Hall et al., 2017). As in Monterey Canyon, net flux from internal tides is up-canyon in some portions of Whittard Canyon (e.g., Amaro et al., 2015, 2016; Aslam et al., 2018). Internal tidal flows focus organic carbon in Whittard Canyon, providing food for benthic communities and submarine

canyon ecosystems (e.g., Huvenne et al., 2011; Amaro et al., 2015). Based on direct comparison of trap and core organic matter measurements at one location in Whittard Canyon by Amaro et al. (2015), organic carbon burial efficiency may exceed specific estimates for Monterey Canyon. Higher organic carbon content in sediment traps (up to 4.5 weight percent) and an overall quieter environment (Amaro et al., 2015) may enhance organic carbon burial efficiency in Whittard Canyon compared with Monterey Canyon.

5.4.2.4. Generalized conceptual model: Based on the results and insights from the novel array of sediment traps along Monterey Canyon, we propose a generalized scheme for organic carbon transport and burial (Fig. 13), which may be representative of transport and mixing processes in submarine canyon environments. Key components of this conceptual model contribute to the sediment accumulation and organic carbon signatures observed in near-seafloor sediment traps. These include primarily marine and terrestrial sources of organic carbon (A) that are effectively mixed along Monterey Canyon (B) by internal tides, which are enhanced near the seafloor (C). Flux of sediment (D) and organic carbon (E) into traps appear to decrease down Monterey Canyon. Water column factors (A–E) occur in conjunction with seafloor exchanges, including internal tide resuspension of fine-grained seafloor sediments (F) and burial of organic carbon (G).

Because our generalized scheme (Fig. 13) is based on intervals dominated by internal tide transport that occur throughout many global submarine canyons (e.g., Shanmugam, 2003; Li et al., 2019), it is possible to extend the process concepts beyond Monterey, Nazaré, and Gaoping (Kaoping) canyons, which are incised through the continental shelf, to submarine canyons that do not experience frequent sediment density flow events. Quantities of, and along-canyon changes in, organic carbon transport, mixing, and burial efficiency will vary based on numerous factors specific to each canyon environment (e.g., Pusceddu et al., 2010).

6. Conclusions

Sediment transport in the axis of Monterey Canyon during intervals between sediment density flow events is dominated by internal tides, which move suspended sediment and organic carbon along the canyon at velocities that increase up-canyon, are enhanced with proximity to the seafloor, and create fine-scale layering in sediment trap samples. Sediment trap samples record composition of organic carbon and fine-grained sediment moving through water column within the submarine canyon, which are not clearly reflected or preserved in canyon deposits. The lack of down-canyon trends in percent modern carbon and organic carbon isotopes ($\delta^{13}\text{C}$, $\delta^{15}\text{N}$) is likely the result of mixing of organic carbon along the canyon, driven by internal tides. Sediment flux into the traps decreases down-canyon, leading to an increase in organic carbon content and xs^{210}Pb activities (dpm/g). Conversely, the rate of organic carbon delivery to the sediment trap (g/day) decreases down-canyon. Measured xs^{210}Pb activities (dpm/g) in traps and seafloor samples increase down-canyon, reflecting lateral transport via internal tides that

may contribute to deposition along the canyon.

Organic carbon content and isotopic signatures in trap samples differ from previous analyses of seafloor samples. The differences between water column and seafloor organic carbon content suggest that organic carbon specific burial efficiency may be low in modern upper Monterey Canyon. Preferential consumption of fresher marine organic carbon, combined with seafloor deposits dominated by sediment density flow event deposits, result in more terrestrial organic carbon isotopic signatures in cores than in sediment trap samples, and may contribute to low first-order organic carbon specific burial efficiency estimates. Our results from an array of sediment traps sampling from the water column between sediment density flow events represent background conditions that are dominated by internal tides. Because internal tidal flow occurs in many submarine canyons globally, we suggest that our detailed results and generalized scheme of organic carbon transport, mixing, and burial developed from Monterey Canyon may be broadly relevant to other submarine canyon settings.

Acknowledgements

Funding for the Coordinated Canyon Experiment (CCE) was provided by David and Lucile Packard Foundation, Natural Environment Research Council (grant NE/K011480/1), U.S. Geological Survey (USGS) Coastal and Marine Program, and Ocean University of China. Funding for radiocarbon analyses was provided by Southern University of Science and Technology. Funding for carbon isotope analyses was provided by MBARI. Funding for ^{210}Pb analyses and CT scanning were provided by USGS. Additional funding for MAC was provided by NERC National Capability CLASS programme (Climate Linked Atlantic Sector Science Programme). CCE data are available in Lundsten (2019) data report. This study would not have been possible without the entire Monterey Coordinated Canyon Experiment (CCE) Team. Special thanks to the USGS Marine Facilities team, especially Cordell Johnson, Dan Powers, Joanne Ferreira, Rob Wyland, Tim Elfers, Pete Dal Ferro, and Jenny White, for operation of sediment traps and upper canyon moorings; Ashley Tuton and University of Southampton grain size facilities; Sharon Borglin and Tim Kneafsey at the Lawrence Berkeley National Laboratory Rock Dynamic and Imaging Lab, and Elliot Kim and Anthony Kavscek at the SUPRI-A Laboratory; Mike Torresan and PCMSC Sediment Laboratories; Dave Mucciarone and Stanford University Stable Isotope Biogeochemistry Lab; MBARI's ship crews, ROV pilots, AUV teams, and CCE shipboard scientific parties.

References

- Alexander, C.R., Venherm, C., 2003. Modern sedimentary processes in the Santa Monica, California continental margin: sediment accumulation, mixing and budget. *Mar. Environ. Res.* 56, 177–204. [http://dx.doi.org/10.1016/S0141-1136\(02\)00330-6](http://dx.doi.org/10.1016/S0141-1136(02)00330-6).
- Amaro, T., de Stigter, H., Lavaleye, M., Duineveld, G., 2015. Organic matter enrichment in the Whittard Channel; its origin and possible effects on benthic megafauna. *Deep-Sea Res. I* 102, 90–100. <http://dx.doi.org/10.1016/j.dsr.2015.04.014>.
- Amaro, T., Huvenne, V.A.I., Allcock, A.L., Aslam, T., Davies, J.S., Danovaro, R., de Stigter, H.C., Duineveld, G.C.A., Gambi, C., Gooday, A.J., Gunton, L.M., Hall, R., Howell, K.L., Ingels, J., Kiriakoulakis, K., Kershaw, C.E., Lavaleye, M.S.S., Robert, K., Steward, H., Van Rooij, D., White, M., Wilson, A.M., 2016. The Whittard Canyon – A case study of submarine canyon processes. *Progr. Oceanogr.* 146, 38–57. <http://dx.doi.org/10.1016/j.pocean.2016.06.003>.
- Anderson, R.Y., 1977. Short term sedimentation response in lakes in western United States as measured by automated sampling. *Limnol. Oceanogr.* 22, 423–433.
- Arzola, R.G., Wynn, R.B., Lastras, G., Masson, D.G., Weaver, P.P.E., 2008. Sedimentary features and processes in the Nazaré and Setúbal submarine canyons, west Iberian margin. *Mar. Geol.* 250, 64–88. <http://doi.org/10.1016/j.margeo.2007.12.006>.
- Aslam, T., Hall, R.A., Dye, S.R., 2018. Internal tides in a dendritic submarine canyon. *Progr. Oceanogr.* <http://dx.doi.org/10.1016/j.pocean.2017.10.005>.
- Baudin, F., Martinez, P., Dennielou, B., Charlier, K., Marsset, T., Droz, L., Rabouille, C., 2017. Organic carbon accumulation in modern sediments of the Angola basin influenced by the Congo deep-sea fan. *Deep-Sea Res. II* 142, 64–74. <http://dx.doi.org/10.1016/j.dsr2.2017.01.009>.
- Bruland, K.W., Franks, R.P., Landing, W.M., Soutar, A., 1981. Southern California inner basin sediment trap calibration. *Earth Planet. Sci. Lett.* 53, 400–408.
- Buesseler, K.O., Antia, A.N., Chen, M., Fowler, S.W., Gardner, W.D., Gustafsson, O., Harada, K., Michaels, A.F., van der Loeff, M.R., Sarin, M., Steinberg, D.K., Trull, T., 2007. An assessment of the use of sediment traps for estimating upper ocean particle fluxes. *J. Mar. Res.* 65, 345–416.

- Butman, C.A., 1986. Sediment trap biases in turbulent flows: Results from a laboratory flume study. *J. Mar. Res.* 44, 645–693.
- Cacchione, D.A., Pratson, L.F., Ogston, A.S., 2002. The shaping of continental slopes by internal tides. *Science* 296, 724–727.
- Campanyà-Llovet, N., Snelgrove, P.V.R., De Leo, F.C., 2018. Food quantity and quality in Barkley Canyon (NE Pacific) and its influence on macroinfaunal community structure. *Progr. Oceanogr.* <http://doi.org/10.1016/j.pocean.2018.04.003>.
- Carter, G.S., Gregg, M.C., 2002. Intense, variable mixing near the head of Monterey Submarine Canyon. *J. Phys. Oceanogr.* 32, 3145–3165.
- Cifuentes, L.A., Sharp, J.H., Fogel, M.L., 1988. Stable carbon and nitrogen isotope biogeochemistry in the Delaware estuary. *Limnol. Oceanogr.* 33, 1102–1115.
- Covault, J.A., Sylvester, Z., Hubbard, S.M., Jobe, Z.R., Sech, R.P., 2016. The stratigraphic record of submarine-channel evolution. *The Sedimentary Record* 14, 4–11. <http://dx.doi.org/10.2110/sedred.2016.3>.
- de Stigter, H.C., Boer, W., de Jesus Mendes, P.A., Jesus, C.C., Thomsen, L., van den Bergh, G.D., van Weering, T.C.E., 2007. Recent sediment transport and deposition in the Nazaré Canyon, Portuguese continental margin. *Mar. Geol.* 246, 144–164. <http://dx.doi.org/10.1016/j.margeo.2007.04.011>.
- Drake, D.E., Gorsline, D.S., 1973. Distribution and transport of suspended particulate matter in Hueneme, Redondo, Newport, and La Jolla submarine canyons, California. *Geolog. Soc. Am. Bull.* 84, 3948–3968.
- Epping, E., van der Zee, C., Soetaert, K., Helder, W., 2002. On the oxidation and burial of organic carbon in sediments of the Iberian margin and Nazaré Canyon (NE Atlantic). *Progr. Oceanogr.* 52, 399–431.
- Farnsworth, K.L., Warrick, J.A., 2007. Sources, dispersal, and fate of fine sediment supplied to coastal California. *U.S. Geolog. Surv. Sci. Investigation Report* 2007-5254, 77 p.
- Fawcett, S.E., Johnson, K.S., Riser, S.C., Van Oostende, N., Sigman, D.M., 2018. Low-nutrient organic matter in the Sargasso Sea thermocline: A hypothesis for its role,

- identity, and carbon cycle implications. *Mar. Chem.*
<http://doi.org/10.1016/j.marchem.2018.10.008>.
- Ferreira, J.T., Rosenberger, K.J., Maier, K.L., 2018. Time-series oceanographic data from the Monterey Canyon, CA October 2015 – March 2017. *U.S. Geol. Surv.*,
<https://doi.org/10.5066/F7FT8J7Q>.
- Fildani, A., Normark, W.R., 2004. Late Quaternary evolution of channel and lobe complexes of Monterey Fan. *Mar. Geol.* 206, 199–223.
<http://dx.doi.org/10.1016/j.margeo.2004.03.001>.
- Fuller, C., Hammond, D.E., 1983. The fallout rate of Pb-210 on the western coast of the United States. *Geophys. Res. Lett.* 10, 1164–1167.
- Galy, V., France-Lanord, C., Beyssac, O., Faure, P., Kudrass, H., Palhol, F., 2007. Efficient organic carbon burial in the Bengal fan sustained by the Himalayan erosional system. *Nature* 450, 407–411. <http://doi.org/10.1038/nature06273>.
- Gardner, W.D., 1980. Sediment trap dynamics and calibration: a laboratory evaluation. *J. Mar. Res.* 38, 17–39.
- Gardner, W.D., 1985. The effect of tilt on sediment trap efficiency. *Deep-Sea Res.* 32, 349–361.
- Gardner, W.D., 1989. Baltimore Canyon as a modern conduit of sediment to the deep sea. *Deep-Sea Res.* 36, 323–358.
- Gardner, W.D., Hinga, K.R., Marra, J., 1983a. Observations on the degradation of biogenic material in the deep ocean with implications on accuracy of sediment trap fluxes. *J. Mar. Res.* 41, 195–214.
- Gardner, W.D., Richardson, M.J., Hinga, K.R., Biscaye, P.E., 1983b. Resuspension measured with sediment traps in a high-energy environment. *Earth Planet. Sci. Lett.* 66, 262–278.
- Gardner, W.D., Biscaye, P.E., Richardson, M.J., 1997. A sediment trap experiment in the Vema Channel to evaluate the effect of horizontal particle fluxes on measured vertical fluxes. *J. Mar. Res.* 55, 995–1028.

- Griggs, G.B., Hein, J.R., 1980. Sources, dispersal, and clay mineral composition of fine-grained sediment off central and northern California. *J. Geology* 88, 541–566.
- Hall, R.A., Carter, G.S., 2011. Internal tides in Monterey Submarine Canyon. *J. Phys. Oceanogr.* 41, 186–204. <http://dx.doi.org/10.1175/2010JPO4471.1>.
- Hall, R.A., Aslam, T., Huvenne, V.A.I., 2017. Partly standing internal tides in a dendritic submarine canyon observed by an ocean glider. *Deep-Sea Res. I*, 126, 73–84. <http://dx.doi.org/10.1016/j.dsr.2017.05.015>.
- Harris, P.T., Whiteway, T., 2011. Global distribution of large submarine canyons: Geomorphic differences between active and passive continental margins. *Mar. Geol.* 285, 69–86. <http://dx.doi.org/10.1016/j.margeo.2011.05.008>.
- He, Y.-B., Lua, J.-X., Li, X.-D., Gao, Z.-Z., Wen, Z., 2011. Evidence of internal-wave and internal-tide deposits in the Middle Ordovician Xujiajuan Formation of the Xiangshan Group, Ningxia, China. *Geo-Mar. Lett.* 31, 509–523. <http://dx.doi.org/10.1007/s00367-011-0253-z>.
- Hedges, J.I., Lee, C., Wakeham, S.G., Hernes, P.J., Peterson, M.L., 1993. Effects of poisons and preservatives on the fluxes and elemental compositions of sediment trap materials. *J. Mar. Res.* 51, 651–668.
- Hotchkiss, F.S., Wunsch, C., 1982. Internal waves in Hudson Canyon with possible geological implications. *Deep-Sea Res.* 29, 415–442.
- Huh, C.-A., Lin, H.-L., Lin, S., Huang, Y.-W., 2009a. Modern accumulation rates and budget of sediment off the Gaoping (Kaoping) River, SW Taiwan: A tidal and flood dominated depositional environment around a submarine canyon. *J. Mar. Sys.* 76, 405–416. <http://doi.org/10.1016/j.jmarsys.2007.07.009>.
- Huh, C.-A., Liu, J.T., Lin, H.-L., Xu, J.P., 2009b. Tidal and flood signatures of settling particles in the Gaoping submarine canyon (SW Taiwan) revealed from radionuclide and flow measurements. *Mar. Geol.* 267, 8–17. <http://dx.doi.org/10.1016/j.margeo.2009.09.001>.
- Hung, G.W., Chung, Y.-C., 1998. Particulate fluxes, ^{210}Pb and ^{210}Po measured from sediment trap samples in a canyon off northeastern Taiwan. *Cont. Shelf Res.* 18, 1475–1491.

- 1019 Huvenne, V.A.I., Tyler, P.A., Masson, D.G., Fisher, E.H., Hauton, C., Hühnerbach, V.,
 1020 Le Bas, T.P., Wolff, G.A., 2011. A picture on the wall: Innovative mapping reveals cold-
 1021 water coral refuge in submarine canyon. PLoS one 6, e28755.
 1022 <https://doi.org/10.1371/journal.pone.0028755>.
 1023
- 1024 Inman, D.L., Jenkins, S.A., 1999. Climate change and the episodicity of sediment flux of
 1025 small California rivers. J. Geology 107, 251–270.
 1026
- 1027 Inman, D.L., Nordstrom, C.E., Flick, R.E., 1976. Currents in submarine canyons: An air-
 1028 sea-land interaction: Ann.Rev. f Fluid Mech. 8, 275–310.
 1029
- 1030 Jingling, Y., Peiliang, L., Cong, L., 2015. Estimating the turbulence characteristics in the
 1031 bottom boundary layer of Monterey Canyon. J. Ocean University of China (Ocean and
 1032 Coastal Sea Research) 14, 210–216. <http://dx.doi.org/10.1007/s11802-015-2456-9>.
 1033
- 1034 Kao, S.-J., Hilton, R.G., Selvaraj, K., Dai, M., Zehetner, F., Huang, J.-C., Hsu, S.-C.,
 1035 Sparkes, R., Liu, J.T., Lee, T.-Y., Yang, J.-Y.T., Galy, A., Xu, X., Hovius, N., 2014.
 1036 Preservation of terrestrial organic carbon in marine sediments offshore Taiwan: mountain
 1037 building and atmospheric carbon dioxide sequestration. Earth Surf. Dynamics 2, 127–
 1038 139. www.earth-surf-dynam.net/2/127/2014.
 1039
- 1040 Kirchner, G., 2011. ^{210}Pb as a tool for establishing sediment chronologies: Examples of
 1041 potentials and limitations of conventional dating methods. J. Environ. Radioact. 102,
 1042 490–494. <http://dx.doi.org/10.1016/j.jenvrad.2010.11.010>.
 1043
- 1044 Krishnaswami, S., Somayajulu, B.L.K., Chung, Y., 1975. $^{210}\text{Pb}/^{226}\text{Ra}$ disequilibrium in
 1045 the Santa Barbara Basin. Earth and Planetary Science Lett. 27, 388–392.
 1046
- 1047 Kudrass, H.R., Michels, K.H., Wiedicke, M., Suckow, A., 1998. Cyclones and tides as
 1048 feeders of a submarine canyon off Bangladesh. Geology 26, 715–718.
 1049
- 1050 Kunze, E., Rosenfeld, L.K., Carter, G.S., Gregg, M.C., 2002. Internal waves in Monterey
 1051 Submarine Canyon. J. Phys. Oceanogr. 32, 1890–1913.
 1052
- 1053 Lee, I-H., Wang, Y.-H., Liu, J.T., Chuang, W.-S., Xu, J., 2009. Internal tidal currents in
 1054 the Gaoping (Kaoping) Submarine Canyon. J. Mar. Sys. 76, 397–404.
 1055 <http://dx.doi.org/10.1016/j.jmarsys.2007.12.011>.
 1056
- 1057 Lehmann, M.F., Bernasconi, S.M., Barbieri, A., McKenzie, J.A., 2002. Preservation of
 1058 organic matter and alteration of its carbon and nitrogen isotope composition during

- 1059 simulated and in situ early sedimentary diagenesis. *Geochem. Cosmochim. Acta* 66,
 1060 3573–3584.
- 1061
- 1062 Lewis, R.C., Coale, K.H., Edwards, B.D., Marot, M., Douglas, J.N., Burton, E.J., 2002.
 1063 Accumulation rate and mixing of shelf sediments in the Monterey Bay National Marine
 1064 Sanctuary. *Mar. Geol.* 181, 157–169.
- 1065
- 1066 Li, M.Z., Prescott, R.H., Robertson, A.G., 2019. Observation of internal tides and
 1067 sediment transport processes at the head of Logan Canyon on central Scotian Slope,
 1068 eastern Canada. *J. Mar. Sys.* 193, 103–125, <https://doi.org/10.1016/j.marsys.2019.01.007>
- 1069
- 1070 Liao, J.-X., Chen, G.-M., Chiou, M.-D., Jan, S., Wei, C.-L., 2017. Internal tides affect
 1071 benthic community structure in an energetic submarine canyon off SW Taiwan. *Deep-Sea*
 1072 *Res. I* 125, 147–160. <http://dx.doi.org/10.1016/j.dsr.2017.05.014>.
- 1073
- 1074 Liu, J.T., Hung, J.-J., Lin, H.-L., Huh, C.-A., Lee, C.-L., Hsu, R.T., Huang, Y.-W., Chu,
 1075 J.C., 2009. From suspended particles to strata: The fate of terrestrial substances in the
 1076 Gaoping (Kaoping) submarine canyon. *Journal of Marine Systems* 76, 417–432.
 1077 <http://dx.doi.org/10.1016/j.jmarsys.2008.01.010>.
- 1078
- 1079 Liu, J.T., Wang, Y.H., Lee, I.-H., Hsu, R.T., 2010. Quantifying tidal signatures of the
 1080 benthic nepheloid layer in Gaoping Submarine Canyon in Southern Taiwan. *Mar. Geol.*
 1081 271, 119–130. <http://dx.doi.org/10.1016/j.margeo.2010.01.016>.
- 1082
- 1083 Liu, J.T., Wang, Y.-H., Yang, R.J., Hsu, R.T., Kao, S.-J., Lin, H.-L., Kuo, F.H., 2012.
 1084 Cyclone-induced hyperpycnal turbidity currents in a submarine canyon. *J. Geophys. Res.*
 1085 117, C04033. <http://dx.doi.org/10.1029/2011JC007630>.
- 1086
- 1087 Liu, J.T., Kao, S.-J., Huh, C.-A., Hung, C.-C., 2013. Gravity flows associated with flood
 1088 events and carbon burial: Taiwan as instructional source area. *Ann. Rev. Mar. Sci.* 5, 47–
 1089 68. <http://dx.doi.org/10.1146/annurev-marine-121211-172307>.
- 1090
- 1091 Liu, J.T., Hsu, R.T., Hung, J.-J., Chang, Y.-P., Wang, Y.-H., Rendle-Bühring, R.H., Lee,
 1092 C.-L., Huh, C.-A., Yang, R.J., 2016. From the highest to the deepest: The Gaoping River
 1093 – Gaoping Submarine Canyon dispersal system. *Earth-Sci. Rev.* 153, 274–300.
 1094 <http://dx.doi.org/10.1016/j.earscirev.2015.10.012>.
- 1095
- 1096 Lundsten, E., 2019. Coordinated Canyon Experiment (CCE) data report. MBARI.org.
 1097 Available at: [https://www.mbari.org/science/seafloor-processes/geological-](https://www.mbari.org/science/seafloor-processes/geological-changes/coordinated-canyon-experiment-datareport-main-page/)
 1098 [changes/coordinated-canyon-experiment-datareport-main-page/](https://www.mbari.org/science/seafloor-processes/geological-changes/coordinated-canyon-experiment-datareport-main-page/)(accessed May 21, 2019).

- 1099
 1100 Maier, K.L., Fildani, A., McHargue, T., Paull, C.K., Graham, S.A., Caress, D.W., 2012,
 1101 Punctuated deep-water channel migration: high-resolution subsurface data from the Lucia
 1102 Chica channel system, offshore California. *J. Sediment. Res.* 82, 1–8.
 1103 <https://dx.doi.org/10.2110/jsr.2012.10>.
 1104
 1105 Maier, K.L., Johnson, S.Y., Hart, P., 2018, Controls on submarine canyon head
 1106 evolution, migration, and fill in Monterey Bay, offshore central California. *Mar. Geol.*
 1107 404, 24–40. <http://dx.doi.org/10.1016/j.margeo.2018.06.014>.
 1108
 1109 Maier, K.L., Gales, J., Paull, C.K., Rosenberger, K., Talling, P.J., Simmons, S.M.,
 1110 Gwiazda, R., McGann, M., Cartigny, M.J.B., Lundsten, E., Anderson, K., Clare, M.A.,
 1111 Xu, J., Parsons, D., Barry, J., Wolfson-Schwehr, M., Nieminski, N., Sumner, E.J., and the
 1112 Monterey Coordinated Canyon Experiment Team, 2019, Linking direct measurements of
 1113 turbidity currents to submarine canyon-floor deposits. *Frontiers in Earth Science:*
 1114 *Sedimentology, Stratigraphy and Diagenesis*, 7, 144,
 1115 <https://doi.org/10.3389/feart.2019.00144>.
 1116
 1117 Martín, J., Palanques, A., Puig, P., 2006. Composition and variability of downward
 1118 particulate matter fluxes in the Palamos submarine canyon (NW Mediterranean). *J. Mar.*
 1119 *Sys.* 60, 75–97. <http://dx.doi.org/10.1016/j.jmarsys.2005.09.010>.
 1120
 1121 Martín, J., Palanques, A., Vitorino, J., Oliveira, A., de Stigter, H.C., 2011. Near-bottom
 1122 particulate matter dynamics in Nazaré submarine canyon under calm and stormy
 1123 conditions. *Deep-Sea Res. II* 58, 2388–2400.
 1124 <http://dx.doi.org/10.1016/j.dsr2.2011.04.004>.
 1125
 1126 Martiny, A.C., Pham, C.T.A., Primeau, F.W., Vrugt, J.A., Moore, J.K., Levin, S.A.,
 1127 Lomas, M.W., 2013. Strong latitudinal patterns in the elemental ratios of marine plankton
 1128 and organic matter. *Nature Geosci.* 6, 279–283. <http://dx.doi.org/10.1038/NGEO1757>.
 1129
 1130 Masson, D.G., Huvenne, V.A.I., de Stigter, H.D., Wolff, G.A., Kiriakoulakis, K., Arzola,
 1131 R.G., Blackbird, S., 2010. Efficient burial of carbon in a submarine canyon. *Geology* 38,
 1132 831–834. <http://dx.doi.org/10.1130/G30895.1>.
 1133
 1134 Matos, F.L., Ross, S.W., Huvenne, V.A.I., Davies, J.S., Cunha, M.R., 2018. Canyons
 1135 pride and prejudice: Exploring the submarine canyon research landscape, a history of
 1136 geographic and thematic bias. *Progr. Oceanogr.*
 1137 <https://doi.org/10.1016/j.pocean.2018.04.010>.
 1138

- 1139 Mountjoy, J.J., Howarth, J.D., Orpin, A.R., Barnes, P.M., Bowden, D.A., Rowden, A.A.,
 1140 Schimel, A.C.G., Holden, C., Horgan, H.J., Nodder, S.D., Patton, J.R., Lamarche, G.,
 1141 Gerstenberger, M., Micallef, A., Pallentin, A., Kane, T., 2018. Earthquakes drive large-
 1142 scale submarine canyon development and sediment supply to deep-ocean basins. *Science*
 1143 *Adv.* 4, eaar3748. <http://dx.doi.org/10.1126/sciadv.aar3748>.
 1144
- 1145 Normark, W., 1970. Channel piracy on Monterey Deep-Sea Fan. *Deep-Sea Res.* 17, 837–
 1146 846.
 1147
- 1148 Palanques, A., El Khatab, M., Puig, P., Masque, P., Sanchez-Cabeza, J.A., Isla, E., 2005.
 1149 Downward particle fluxes in the Guadiaro submarine canyon depositional system (north-
 1150 western Alboran Sea), a river flood dominated system. *Mar. Geol.* 220, 23–40.
 1151 <http://dx.doi.org/10.1016/j.dsr.2008.11.002>.
 1152
- 1153 Paull, C.K., Ussler, W. III, Greene, H.G., Keaten, R., Mitts, P., Barry, J., 2003. Caught in
 1154 the act: The 20 December 2001 gravity flow event in Monterey Canyon. *Geo-Ma. Lett.*
 1155 22, 227–232. <http://dx.doi.org/10.1007/s00367-003-0117-2>.
 1156
- 1157 Paull, C.K., Mitts, P., Ussler, W. III, Keaten, R., Greene, H.G., 2005. Trail of sand in
 1158 upper Monterey Canyon: Offshore California. *Geol. Soc. Am. Bull.* 117, 1134–1145.
 1159 <http://dx.doi.org/10.1130/B25390.1>.
 1160
- 1161 Paull, C.K., Ussler, W. III, Mitts, P.J., Caress, D.W., West, G.J., 2006. Discordant ¹⁴C-
 1162 stratigraphies in upper Monterey Canyon: A signal of anthropogenic disturbance. *Mar.*
 1163 *Geol.* 233, 21–36. <http://dx.doi.org/10.1016/j.margeo.2006.07.008>.
 1164
- 1165 Paull, C.K., Ussler, W. III, Caress, D.W., Lundsten, E., Covault, J.A., Maier, K.L., Xu, J.,
 1166 Augenstein, S., 2010a. Origins of large crescent-shaped bedforms within the axial
 1167 channel of Monterey Canyon, offshore California. *Geosphere* 6, 1–20.
 1168 <http://dx.doi.org/10.1130/GES00527.1>.
 1169
- 1170 Paull, C.K., Schlining, B., Ussler, W. III, Lundsten, E., Barry, J.P., Caress, D.W.,
 1171 Johnson, J.E., McGann, M., 2010b. Submarine mass transport within Monterey Canyon:
 1172 Benthic disturbance controls on the distribution of chemosynthetic biologic communities,
 1173 in Mosher, D.C. et al. (eds) *Submarine Mass Movements and Their Consequences*,
 1174 Springer, Dordrecht. *Advances in Natural and Technological Hazards Research* 28, 229–
 1175 246. http://dx.doi.org/10.1007/978-90-481-3071-9_19.
 1176
- 1177 Paull, C.K., Caress, D.W., Ussler, W. III, Lundsten, E., Meiner-Johnson, M., 2011. High-
 1178 resolution bathymetry of the axial channels within Monterey and Soquel submarine
 1179 canyons, offshore central California. *Geosphere* 7, 1077–1101.
 1180 <http://dx.doi.org/10.1130/GES00636.1>.

- 1181
 1182 Paull, C.K., Talling, P.J., Maier, K.L., Parsons, D., Xu, J., Caress, D.W., Gwiazda, R.,
 1183 Lundsten, E., Anderson, K., Barry, J., Chaffey, M., O'Reilly, T., Rosenberger, K.,
 1184 Simmons, S.M., McCann, M., McGann, M., Kieft, B., Gales, J., Sumner, E.J., Clare,
 1185 M.A., Cartigny, M.J., Monterey Coordinated Canyon Experiment Team, 2018. Powerful
 1186 turbidity currents driven by dense basal layers. *Nature Comm.* 9, 4114.
 1187 <http://dx.doi.org/10.1038/s41467-018-06254-6>.
 1188
 1189 Peters, K.E., Sweeney, R.E., Kaplan, I.R., 1978. Correlation of carbon and nitrogen
 1190 stable isotope ratios in sedimentary organic matter. *Limnol. Oceanogr.* 23, 598–604.
 1191
 1192 Petruncio, E.T., Rosenfeld, L.K., Paduan, J.D., 1998. Observations of the internal tide in
 1193 Monterey Canyon. *J. Phys. Oceanogr.* 28, 1873–1903.
 1194
 1195 Petruncio, E.T., Paduan, J.D., Rosenfeld, L.K., 2002. Numerical simulations of the
 1196 internal tide in a submarine canyon. *Ocean Model.* 4, 221–248.
 1197
 1198 Pomar, L., Morsilli, M., Hallock, P., Bádenas, B., 2012. Internal waves, an under-
 1199 explored source of turbulence events in the sedimentary record. *Earth-Sci. Rev.* 111, 56–
 1200 81. <http://dx.doi.org/10.1016/j.earscirev.2011.12.005>.
 1201
 1202 Pusceddu, A., Bianchelli, S., Canals, M., Sanchez-Vidal, A., Durrieu De Madron, X.D.,
 1203 Heussner, S., Lykousis, V., de Stigter, H., Trincardi, F., Danovaro, R., 2010. Organic
 1204 matter in sediments of canyons and open slopes of the Portuguese, Catalan, Southern
 1205 Adriatic and Cretan Sea margins. *Deep-Sea Res. I* 57, 441–457.
 1206 <http://doi.org/10.1016/j.dsr.2009.11.008>.
 1207
 1208 Prouty, N.G., Mienis, F., Campbell-Swarzenski, P., Roark, E.B., Davies, A.J., Robertson,
 1209 C.M., Duineveld, G., Ross, S.W., Rhode, M., Demopoulos, A.W.J., 2017. Seasonal
 1210 variability in the source and composition of particulate matter in the depositional zone of
 1211 Baltimore Canyon, U.S. Mid-Atlantic Bight. *Deep-Sea Res. I* 127, 77–89.
 1212 <http://dx.doi.org/10.1016/j.dsr.2017.08.004>.
 1213
 1214 Rau, G.H., Chavez, F.P., Friederich, G.E., 2001. Plankton $^{13}\text{C}/^{12}\text{C}$ variations in
 1215 Monterey Bay, California: evidence of non-diffusive inorganic carbon uptake by
 1216 phytoplankton in an upwelling environment. *Deep-Sea Res. I* 48, 79–94.
 1217
 1218 Redfield, A., 1934. James Johnstone Memorial Volume 176–192, Liverpool University
 1219 Press.
 1220

- Rendigs, R.R., Anderson, R.Y., Xu, J., Davis, R.E., Bergeron, E., 2009. The partition intervalometer: A programmable underwater timer for marking accumulated sediment profiles collected in Anderson sediment traps: Development, operation, testing procedures, and field results. U.S. Geol. Surv. Open-File Report 2009-1101. <https://pubs.usgs.gov/of/2009/1101>.
- Romero-Romero, S., Molina-Ramírez, A., Höfer, J., Duinveld, G., Rumín-Caparrós, A., Sanchez-Vidal, A., Canals, M., Acuña, J.L., 2016. Seasonal pathways of organic matter within the Avilés submarine canyon: Food web implications. *Deep-Sea Res. I* 117, 1–10. <http://dx.doi.org/10.1016/j.dsr.2016.09.003>.
- Rosenberger, K.J., Storlazzi, C.D., Cheriton, O.M., 2016. Variability of the internal tide on the southern Monterey Bay continental shelf and associated bottom boundary layer sediment transport. *Cont. Shelf Res.* 120, 68–81. <http://dx.doi.org/10.1016/j.csr.2016.03.016>.
- Shanmugam, G., 2003. Deep-marine tidal bottom currents and their reworked sands in modern and ancient submarine canyons. *Mar. Petrol. Geol.* 20, 471–491. [http://dx.doi.org/10.1016/S0264-8172\(03\)00063-1](http://dx.doi.org/10.1016/S0264-8172(03)00063-1).
- Shea, R.E., Broenkow, W.W., 1982. The role of internal tides in the nutrient enrichment of Monterey Bay, California. *Estuarine, Coastal Shelf Sci.* 15, 57–66.
- Shepard, F.P., 1976. Tidal components of currents in submarine canyons. *J. Geol.* 84, 343–350.
- Shepard, F.P., 1979. Currents in submarine canyons and other types of sea valleys. *SEPM Sp. Pub. No. 27*, 85–94.
- Shepard, F.P., Marshall, N.F., 1969. Currents in La Jolla and Scripps submarine canyons. *Science* 165, 177–178. <http://dx.doi.org/10.1126/science.165.3889.177>.
- Smith, D.P., Ruiz, G., Kvitek, R., Iampietro, P.J., 2005. Semiannual patterns of erosion and deposition in upper Monterey Canyon from serial multibeam bathymetry. *Geol. Soc. Am. Bull.* 117, 1123–1133. <http://dx.doi.org/10.1130/B25510.1>.
- Smith, D.P., Kvitek, R., Iampietro, P.J., Wong, K., 2007. Twenty-nine months of geomorphic change in upper Monterey Canyon (2002–2005). *Mar. Geol.* 236, 79–94. <http://dx.doi.org/10.1016/j.margeo.2006.09.024>.

- 1261 Smoak, J.M., Moore, W.S., Thunell, R.C., 2000. Influence of boundary scavenging and
 1262 sediment focusing on ^{234}Th , ^{228}Th and ^{210}Pb fluxes in the Santa Barbara Basin. *Estuarine,*
 1263 *Coastal Shelf Sci.* 51, 373–384.
 1264
- 1265 Stevens, T., Paull, C.K., Ussler, W. III, McGann, M., Buylaert, J.-P., Lundsten, E., 2014.
 1266 The timing of sediment transport down Monterey Submarine Canyon, offshore
 1267 California. *Geol. Soc. Am. Bull.* 126, 103–121. <http://dx.doi.org/10.1130/B30931.1>.
 1268
- 1269 Stuiver, M., Polach, H.A., 1977. Discussion: Reporting on ^{14}C date, *Radiocarbon* 19,
 1270 855–858.
 1271
- 1272 Swarzenski, P.W., 2014. ^{210}Pb dating. In: Rink, W., Thompson, J. (Eds.), *Encyclopedia*
 1273 *of Scientific Dating Methods*. Springer, Dordrecht, pp 1–11.
 1274 <http://dx.doi.org/10.1007/978-94-007-6326-5>.
 1275
- 1276 Swarzenski, P.W., Baskaran, M., Rosenbauer, R.J., Oren, W.H., 2006. Historical trace
 1277 element distribution in sediments from the Mississippi River Delta. *Estuaries and Coasts*
 1278 29, 1094–1107.
 1279
- 1280 Symons, W.O., Sumner, E.J., Paull, C.K., Cartigny, M.J.B., Xu, J.P., Maier, K.L.,
 1281 Lorenson, T.D., Talling, P.J., 2017. A new model for turbidity current behavior based on
 1282 integration of flow monitoring and precision coring in a submarine canyon. *Geology* 45,
 1283 367–370. <http://dx.doi.org/10.1130/G38764.1>.
 1284
- 1285 Talling, P.J., Allin, J., Armitage, D.A., Arnott, R.W.C., Cartigny, M.J.B., Clare, M.A.,
 1286 Felletti, F., Covault, J.A., Girardclos, S., Hansen, E., Hill, P.R., Hiscott, R.N., Hogg, A.J.,
 1287 Hughes Clarke, J., Jobe, Z.R., Malgesini, G., Mozzato, A., Naruse, H., Parkinson, S.,
 1288 Peel, F.J., Piper, D.J.W., Pope, E., Postmas, G., Rowley, P., Sguazzini, A., Stevenson,
 1289 C.J., Sumner, E.J., Sylvester, Z., Watts, C., Xu, J., 2015. Key future directions for
 1290 research on turbidity currents and their deposits. *J. Sed. Res.* 85, 153–169.
 1291 <http://dx.doi.org/10.2110/jsr.2015.03>.
 1292
- 1293 van Oevelen, D., Soetaert, K., Garcia, R., de Stigter, H.C., Cunha, M.R., Pusceddu, A.,
 1294 Danovaro, R., 2011. Canyon conditions impact carbon flows in food webs of three
 1295 sections of the Nazaré canyon. *Deep-Sea Res. II* 58, 2461–2476.
 1296 <http://doi.org/10.1016/j.dsr2.2011.04.009>.
 1297
- 1298 Vendettuoli, D., Clare, M.A., Hughes Clarke, J.E., Vellinga, A., Hizzett, J., Hage, S.,
 1299 Cartigny, M., Talling, P.J., Waltham, D., Hubbard, S., Stacey, C., Lintern D.G., 2019.
 1300 Daily bathymetric surveys document how stratigraphy is built and its extreme

- 1301 incompleteness in submarine channels. *Earth Planet. Sci. Lett.* 515, 231–247.
 1302 <https://doi.org/10.1016/j.epsl.2019.03.033>.
 1303
- 1304 Wain, D.J., Gregg, M.C., Alford, M.H., Lien, R.-C., Hall, R.A., Carter, G.S., 2013.
 1305 Propagation and dissipation of the internal tide in upper Monterey Canyon. *J. Geophys.*
 1306 *Res. Oceans* 118, 4855–4877. <http://dx.doi.org/10.1002/jgrc.20368>.
 1307
- 1308 Wang, X., Chao, Y., Dong, C., Farrara, J., Li, Z., McWilliams, J.C., Paduan, J.D.,
 1309 Rosenfeld, L.K., 2009. Modeling tides in Monterey Bay, California. *Deep-Sea Res. II* 56,
 1310 219–231. <http://dx.doi.org/10.1016/j.dsr2.2008.08.012>.
 1311
- 1312 Waterhouse, A.F., Mackinnon, J.A., Musgrave, R.C., 2017. Internal tide convergence and
 1313 mixing in a submarine canyon. *J. Phys. Oceanogr.* 47, 303–322.
 1314 <http://dx.doi.org/10.1175/JPO-D-16-0073.1>.
 1315
- 1316 Xu, J.P., Noble, M.A., 2009. Currents in Monterey Submarine Canyon. *J. Geophys. Res.*
 1317 114, C03004. <http://dx.doi.org/10.1029/2008JC004992>.
 1318
- 1319 Xu, J.P., Noble, M., Eittreim, S.L., 2002a. Suspended sediment transport on the
 1320 continental shelf near Davenport, California. *Mar. Geol.* 181, 171–193.
 1321
- 1322 Xu, J.P., Noble, M., Eittreim, S.L., Rosenfeld, L.K., Schwing, F.B., Pilskalns, C.H.,
 1323 2002b. Distribution and transport of suspended particulate matter in Monterey Canyon,
 1324 California. *Mar. Geol.* 181, 215–234.
 1325
- 1326 Xu, J.P., Wong, F.L., Kvitek, R., Smith, D.P., Paull, C.K., 2008. Sandwave migration in
 1327 Monterey Submarine Canyon, central California. *Mar. Geol.* 248, 193–212.
 1328 <http://dx.doi.org/10.1016/j.margeo.2007.11.005>.
 1329
- 1330 Xu, J.P., Swarzenski, P.W., Noble, M., Li, A.-C., 2010. Event-driven sediment flux in
 1331 Hueneme and Mugu submarine canyons, southern California. *Mar. Geol.* 269, 74–88.
 1332 <http://dx.doi.org/10.1016/j.margeo.2009.12.007>.
 1333
- 1334 Xu, J.P., Sequeiros, O.E., Noble, M.A., 2014. Sediment concentrations, flow conditions,
 1335 and downstream evolution of two turbidity currents, Monterey Canyon, USA. *Deep-Sea*
 1336 *Res. I* 89, 11–34. <http://dx.doi.org/10.1016/j.dsr.2014.04.001>.
 1337
- 1338 Yang, W., Guo, L., Chuang, C.-Y., Santschi, P.H., Schumann, D., Ayranov, M., 2015.
 1339 Influence of organic matter on the adsorption of ^{210}Pb , ^{210}Po and ^7Be and their

- fractionation on nanoparticles in seawater. *Earth Planet. Sci. Lett.* 423, 193–201.
<http://dx.doi.org/10.1016/j.epsl.2015.05.007>.
- Zheng, L.-W., Ding, X., Liu, J.T., Li, D., Lee, T.-Y., Zheng, X., Zheng, Z., Xu, M.N., Dai, M., Kao, S.-J., 2017. Isotopic evidence for the influence of typhoons and submarine canyons on the sourcing and transport behavior of biospheric organic carbon to the deep sea. *Earth Planet. Sci. Lett.* 465, 103–111. <http://dx.doi.org/10.1016/j.epsl.2017.02.037>.
- Zhenzhong, G., Eriksson, K.A., 1991. Internal-tide deposits in an Ordovician submarine channel: Previously unrecognized facies? *Geology* 19, 734–737.
- Zúñiga, D., Flexas, M.M., Sanchez-Vidal, A., Coenjaerts, J., Calafat, A., Jordà, G., García-Orellana, J., Puigdefàbregas, J., Canals, M., Espino, M., Sardà, F., Company, J.B., 2009. Particle fluxes dynamics in Blanes submarine canyon (Northwestern Mediterranean). *Prog. Oceanogr.* 82, 239–251. <http://dx.doi.org/10.1016/j.pocean.2009.07.002>.

Tables

Table 1. Anderson-type sediment trap deployments.

Table 2. Summary of ADCP current velocities.

Figures

Fig. 1. Map of study area in Monterey Canyon, offshore central California. Blue squares indicate locations of CCE moorings (MS#). Dashed arrows depict littoral transport paths into Monterey Canyon. WHS: wave height sensor. Modified from Paull et al. (2018).

Fig. 2. Schematic illustrations of moorings and sediment traps deployed in the Coordinated Canyon Experiment in Monterey Canyon. (A) Schematic representation of an Anderson-type sediment trap deployed on mooring (not to scale) (modified from Paull et al., 2018). ADCP: acoustic Doppler current profiler. masf: meters above the seafloor. (B) Schematic Anderson-type sediment trap (not to scale) filling with sediment between times t_1 and t_2 .

Fig. 3. Correlation of sediment trap samples with computed tomography (CT) scan and grain size plots. Trap names contain mooring (MS#), type of sediment trap (AST), meters above the seafloor (##m), and numeric deployment date (year month day). Trap tubes shown as abbreviated datasets of CT scan coronal images (shaded individually to highlight features) and grain size analyses (d0.1:red; D[4,3]:black; d0.9:gray; see Supplementary Table 1 and Lundsten, 2019). Disc dates are shown as numeric month and day. (A) Deployment I. (B) Deployment II. (C) Deployment III. (D) Enlarged portions of CT images highlighting fine-scale layering in the upper canyon traps.

Fig. 4. Grain size distribution plots of background sediment (averaged fine-grained, non-sediment density flow event intervals) in Anderson-type sediment traps. Trap names as in Figure 3. masf: meters above the seafloor. (A) Deployment I. (B) Deployment II. (C) Deployment III.

Fig. 5. Plots of radiocarbon analyses (see Supplementary Table 2). masf: meters above the seafloor. (A) Percent modern carbon (pMC) plotted with mooring water depth. (B) pMC results normalized for apparent sediment flux into the traps.

Fig. 6. Organic carbon content (see Supplementary Table 3). (A) Weight percent (wt. %) total organic carbon (TOC) plotted with mooring water depth. (B) TOC flux.

Fig. 7. Organic carbon stable isotopes (see Supplementary Table 3). masf: meters above the seafloor. (A) $\delta^{13}\text{C}$ plotted with mooring water depth. (B) Plot of $\delta^{15}\text{N}$ and $\delta^{13}\text{C}$.

Fig. 8. Excess (xs) ^{210}Pb activities (see Supplementary Table 4). (A) xs ^{210}Pb activities

plotted with sediment trap water depth. masf: meters above the seafloor. (B) $x_s^{210}\text{Pb}$ activities normalized for apparent sediment flux into traps. (C) Plot of $x_s^{210}\text{Pb}$ activities and total organic carbon (TOC) from the same sediment traps.

Fig. 9. Internal tide at MS1. (A) Profiles from a downward-looking 300 kHz acoustic Doppler current profiler (ADCP) showing semi-diurnal velocity variations oriented up-canyon (positive) and down-canyon (negative) at 10 meters above the seafloor (masf; red) and 65 masf (blue) from November 26 – December 6, 2015. Internal tide velocities increase near the seafloor and reach up to 1 m/s oriented up-canyon at 10 masf. (B) Semi-diurnal turbidity oscillations from a sensor at 35 masf during the same period as Part A. Solid gray lines between plots in Part A and Part B highlight spikes in turbidity at 35 masf coinciding with spikes in velocity at 10 or 65 masf, and dashed gray lines highlight spikes in turbidity at 35 masf coinciding with periods of low velocities at 10 and (or) 65 masf where internal tide orientation switches. (C) November 30, 2015, ADCP measurements of an up-canyon internal tide.

Fig. 10. Suspended sediment estimation for the first 16 days (32 tidal cycles) of Deployment III at MS1, MS2, and MS3. Dates are shown as numeric year month day. (A) Along-canyon velocity at 10 meters above the seafloor (masf) measured from a downward-looking ADCP at 65 masf. Positive velocities are oriented up-canyon, and negative velocities are oriented down-canyon. (B) Suspended sediment concentration converted from transmissometer beam attenuation using fine-grained background sediment in this study and the calibration of Xu et al. (2002a). (C) Suspended sediment flux calculated from Parts (A) and (B).

Fig. 11. Additional sandy layers at MS1. (A, E) Sediment trap CT images (see Fig. 3), (B, F) wave height (H10 – top 10th percentile of wave height measurements), (C, G) mean wave direction (blue; average of wave spectrum weighted by energy) and peak period direction (red), and (D, H) turbidity at MS1 measured 35 meters above the seafloor from (A–D) Deployment I November 22–30, 2015 and (E–H) Deployment III November 7–15, 2016. Stars (A, E) indicate sandy units that do not correspond to sediment density flow events or strong up-canyon internal tide events; they appear to coincide with intervals of increased wave height oriented towards the southeast to northeast.

Fig. 12. Comparison of seafloor sediment core samples and sediment trap analyses. (A) $\delta^{13}\text{C}$. Trap samples generally show equal or depleted $\delta^{13}\text{C}$ signatures compared with canyon seafloor deposits. (B) $\delta^{13}\text{C}$ and $\delta^{15}\text{N}$. Core samples have depleted $\delta^{13}\text{C}$ and $\delta^{15}\text{N}$ values compared with sediment trap samples (simplified marine and terrestrial signatures after Peters et al., 1978; Paull et al., 2006). (C) Total organic carbon (TOC). Sediment

traps consistently contain more organic carbon than deposits from similar canyon water depths. (D) Plot of $x_s^{210}\text{Pb}$ activities in sediment traps (this study; plotted as sediment trap water depth) and the top centimeter (0–1 cm below the seafloor) from Monterey Canyon push core samples adjacent to the axial channel (Symons et al., 2017; unpublished data, courtesy of T. Lorenson). $x_s^{210}\text{Pb}$ activities increase down canyon in both sample sets, with push core seafloor values consistently equal to or lower than traps at 10+ m above the seafloor.

Fig. 13. Schematic summary of submarine canyon sediment and organic carbon transport and deposition along a down-canyon-axis profile. Key components noted (letters), with Monterey Canyon examples italicized. Sizes of labels and lines are broadly representative of the relative quantity and importance of processes down the canyon. Not to scale. mwd: meters water depth. ADCP: acoustic Doppler current profiler. OMZ: oxygen minimum zone.

Supplementary Tables

Supplementary Table 1. Laser particle grain size summary.

Supplementary Table 2. Radiocarbon analyses.

Supplementary Table 3. Organic carbon content and stable isotope analyses.

Supplementary Table 4. ^{210}Pb analyses.

Table 1. Anderson-type sediment trap deployments.

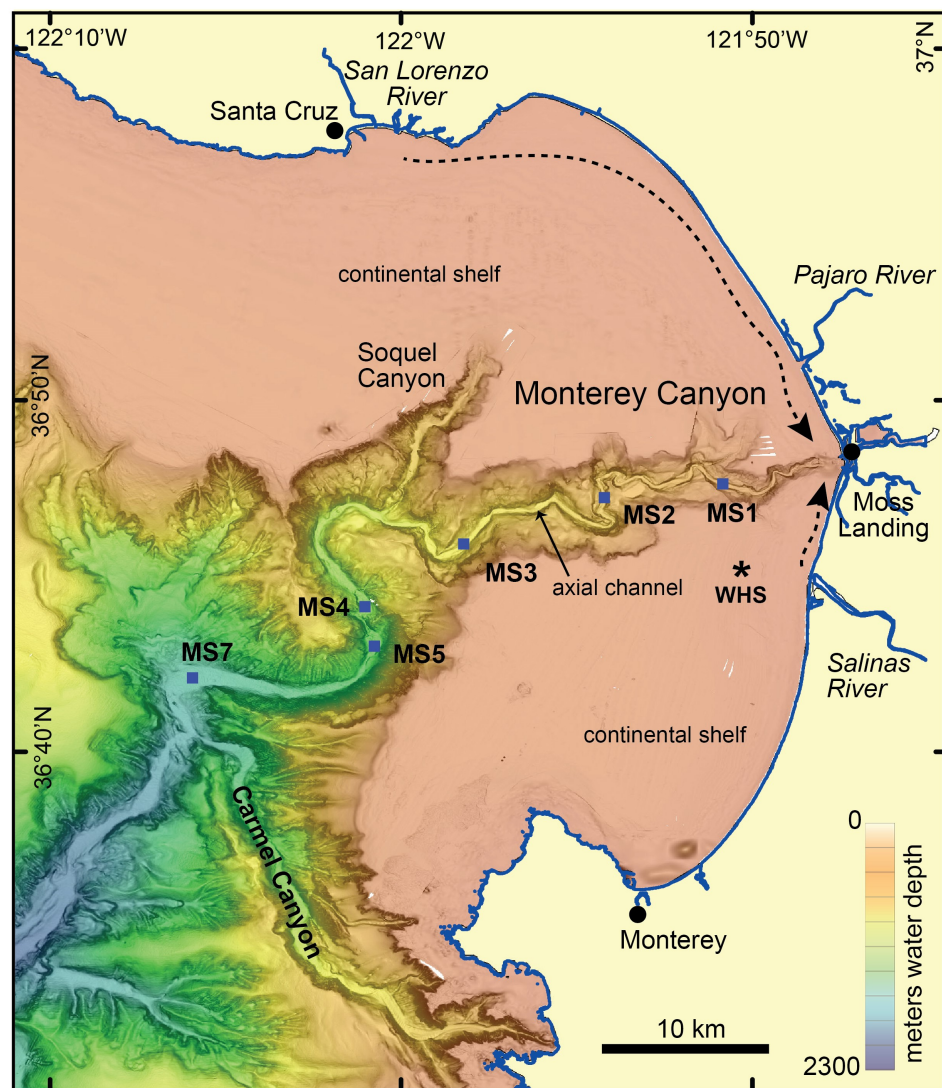
Deployment	Mooring	Mooring Water Depth (m)	Sediment Trap Position (masf) ¹	Latitude	Longitude	Deployed ²	Recovered ²	Sediment Trap Status at Recovery	Total 1-cm Slices	Date ² of First Sediment Density Flow Event in Trap ⁴	Background Sediment Accumulated (cm) ⁵	Average Apparent Sediment Accumulation Rate (g/m ² /day)	Intervalometer Sediment Accumulation Rate (g/m ² /day) ⁶
I	MS1	287	10	36.793280	-121.844600	20151006	N/A	ripped off	N/A	N/A	N/A	N/A	N/A
I	MS1	287	35	36.793280	-121.844600	20151006	20160117	overflow	79	20151201	79	460	450 ±187
I	MS2	527	10	36.788270	-121.903400	20151005	20160405	overflow	80	20160115	80	380	398 ±158
I	MS3	831	10	36.764970	-121.969700	20151005	20160405	overflow	89	20160115	77	440	400 ±169
I	MS4	1286	10	36.735795	-122.016478	20151007	20160405	overflow	95	20160115	60	220	N/A
I	MS5	1449	11	36.714960	-122.013000	20151020	20160405	overflow	95	20160115	32	180	164 ±57
I	MS5	1449	74	36.714960	-122.013000	20151020	20160405	overflow	91	20160115	26	120	N/A
I	MS7	1849	10	36.701620	-122.097500	20151027	20160412	full	87	20160115	10	40	N/A
I	MS7	1849	300	36.701620	-122.097500	20151027	20160412	underfilled	9	N/A	9	20	N/A
II	MS1	278	10	36.793240	-121.844716	20160404	20161003	overflow	93	20160901	86	220	N/A
II	MS2	527	10	36.787832	-121.903508	20160407	20161003	overflow	95	20160901	95	400	383 ±206
II	MS3	822	10	36.764763	-121.969575	20160407	20161004	overflow	89	20160901	89	460	503 ±195
II	MS4	1285	10	36.736000	-122.016667	20160408	20161004	overflow	97	20160901	96	240	N/A
II	MS5	1445	11	36.715517	-122.012875	20160408	20161004	overflow	91	20160901	64	160	N/A
II	MS5	1445	74	36.715517	-122.012875	20160408	20161004	full	74	20160901	52	140	N/A
II	MS7	1849	10	36.701784	-122.098400	20160420	20161010	full ³	N/A	N/A	N/A	N/A	N/A
II	MS7	1849	300	36.701784	-122.098400	20160420	20161010	underfilled	19	N/A	19	40	N/A
III	MS1	290	10	36.793557	-121.845658	20161006	20170321	full	77	20161124	66	620	618 ±289
III	MS1	290	35	36.793557	-121.845658	20161006	20170321	underfilled	13	20161124	N/A	N/A	N/A
III	MS2	523	10	36.787250	-121.903383	20161006	N/A	ripped off	N/A	N/A	N/A	N/A	N/A
III	MS3	817	10	36.765045	-121.969880	20161006	20170321	overflow	96	20161124	38	300	307 ±74
III	MS3	817	35	36.765045	-121.969880	20161006	20170321	overflow	89	20161124	38	300	N/A
III	MS4	1263	10	36.735898	-122.016470	20161007	20170322	overflow	80	20170122	80	280	N/A
III	MS5	1439	11	36.716333	-122.012833	20161007	20170206	overflow	87	20170122	65	220	238 ±92
III	MS5	1439	74	36.716333	-122.012833	20161007	20170206	overflow	84	20170122	48	180	N/A
III	MS7	1849	10	36.701549	-122.098372	20161019	20170404	full	67	20170203	32	120	N/A
III	MS7	1849	300	36.701549	-122.098372	20161019	20170404	underfilled	24	N/A	24	60	N/A

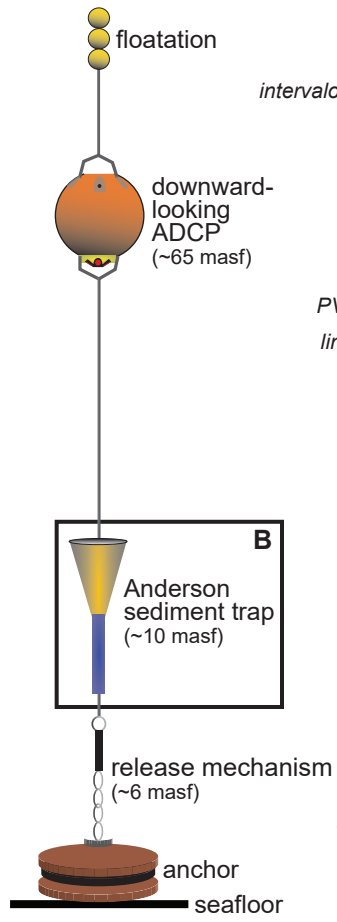
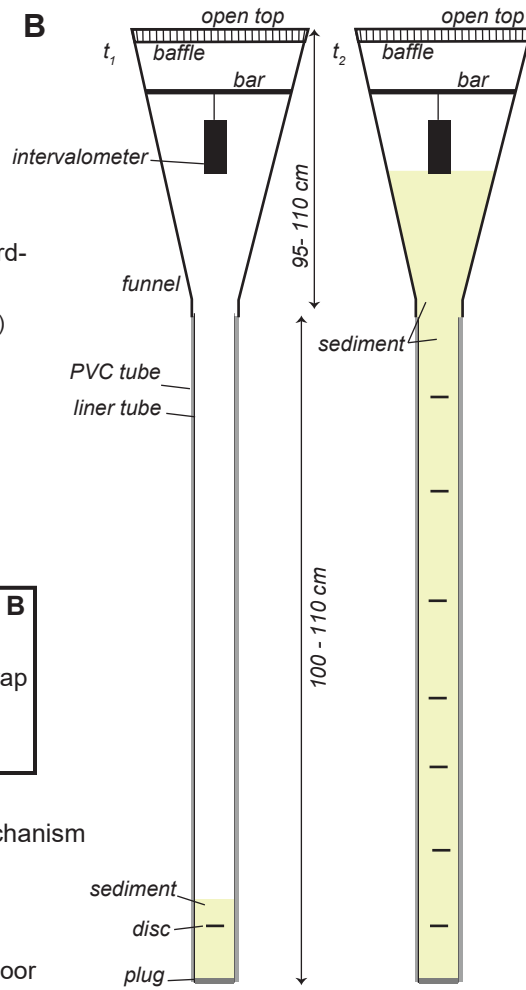
¹masf: meters above the seafloor²dates shown as year, month, day³material recovered but not stratigraphy⁴see Paull et al. (2018)⁵calculated from intervalometer discs, CT scans and grain size data⁶shown as averages and single standard deviation

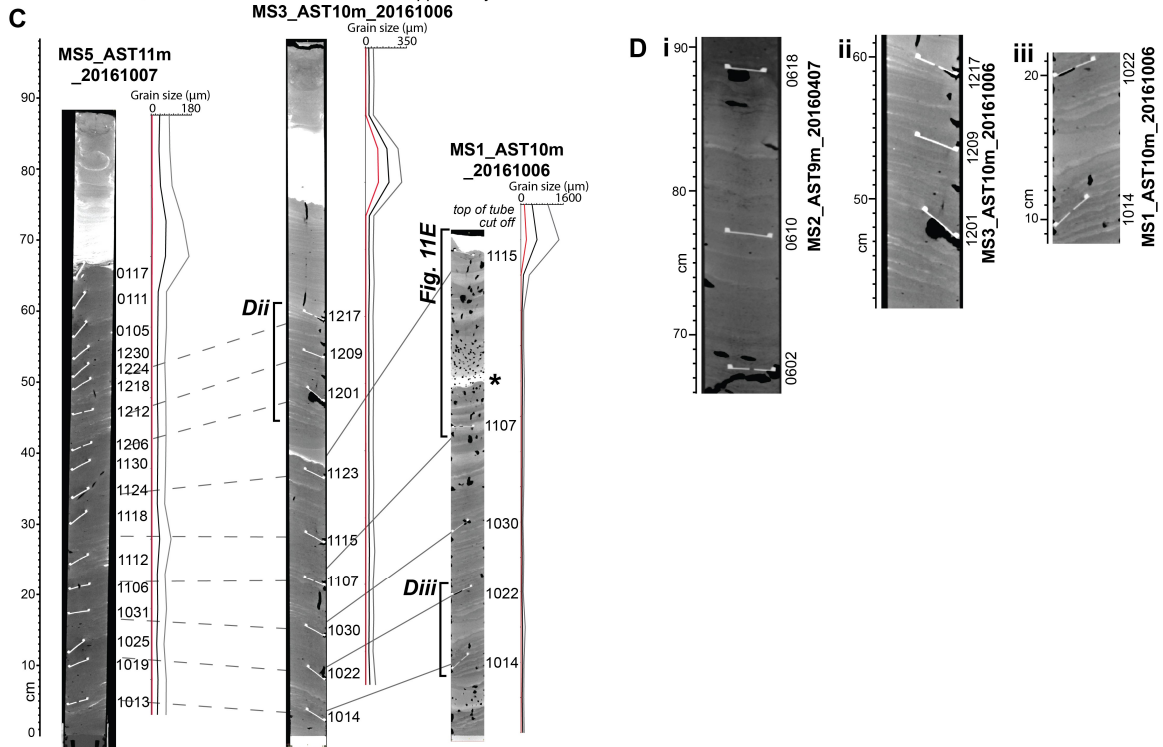
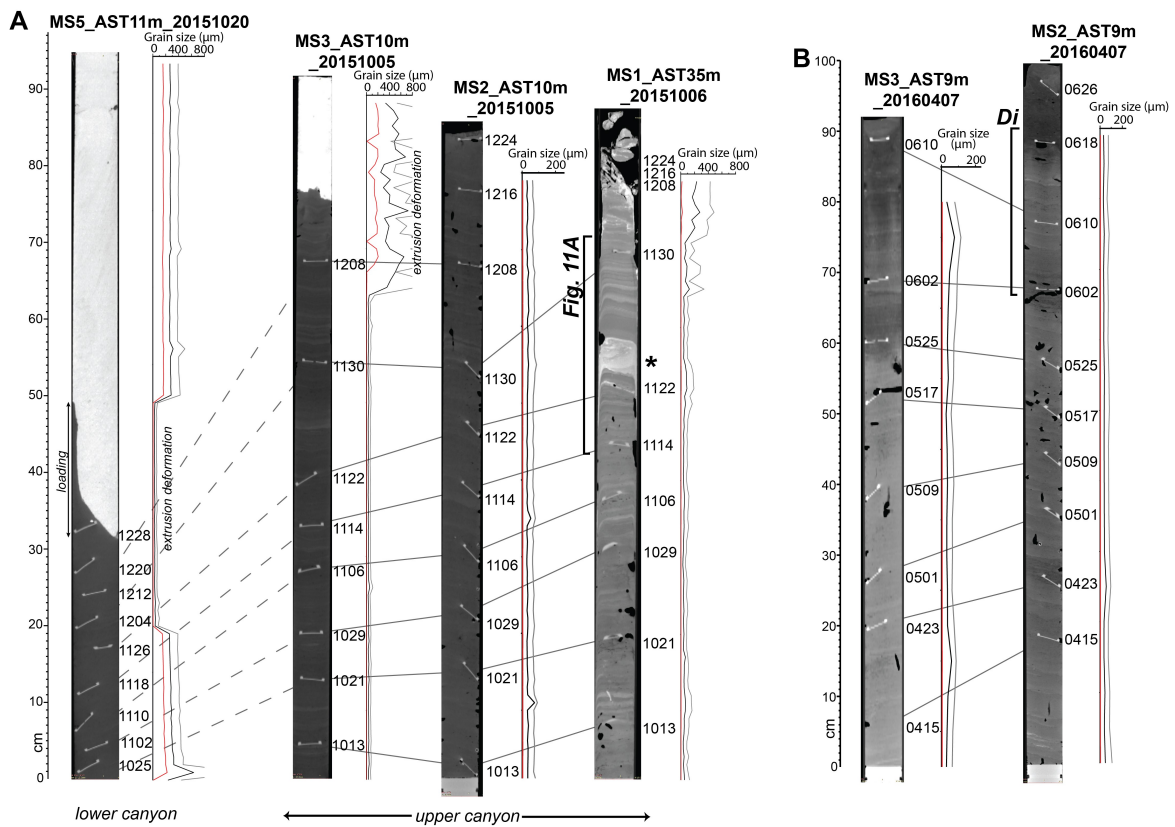
Table 2. Summary of ADCP current velocities.

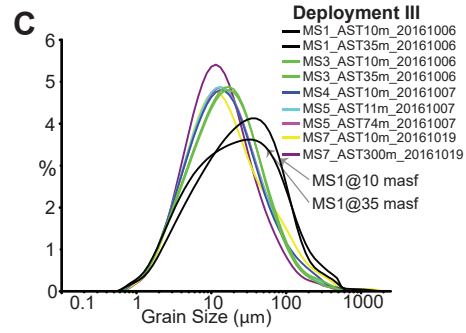
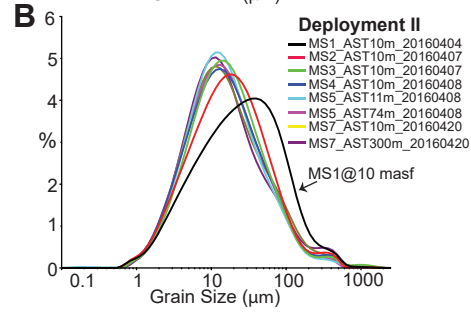
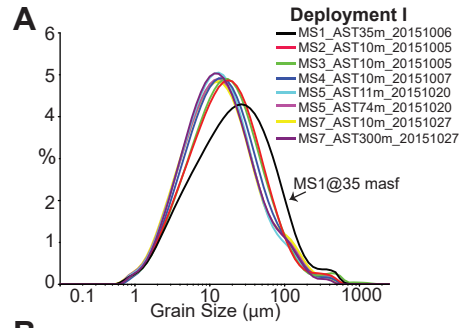
Deployment ¹	Mooring	<i>Statistics</i>		<i>Distribution (% deployment time)</i>						
		Mean (cm/s)	Standard Deviation (cm/s)	0–10 cm/s	10–20 cm/s	20–30 cm/s	30–40 cm/s	40–50 cm/s	50–60 cm/s	60–70 cm/s
II	MS1	19.4	11.8	24.2	34.1	23.1	12.3	4.7	1.3	0.2
III	MS1	17.5	11.6	29.1	36.5	20.9	9.1	3.1	0.8	0.2
II	MS2	17.1	10.5	28.5	38.1	21.0	8.5	2.7	0.6	0.1
III	MS2	15.1	9.4	31.5	41.3	17.8	4.3	0.9	0.3	0.1
II	MS3	13.6	8.0	36.8	43.7	15.3	3.0	0.4	0.1	0
III	MS3	16.6	10.7	30.3	37.8	20.9	8.3	2.1	0.3	0.1
II	MS4	13	7.4	39.8	43.0	14.0	2.3	0.2	<0.1	<0.1
III	MS4	16.7	9.4	26.1	39.7	23.4	7.2	1.2	0.2	0.1
II	MS5	12.4	7.3	42.0	44.1	11.4	1.9	0.3	<0.1	<0.1
III	MS5	15.9	9.8	31.0	41.3	18.0	7.2	2.0	0.3	0.1
II	MS7	17.7	10.1	23.9	40.7	22.8	9.0	2.9	0.5	<0.1
III	MS7	19.8	11.1	20.2	36.1	25.7	12.6	4.3	1.0	0.1

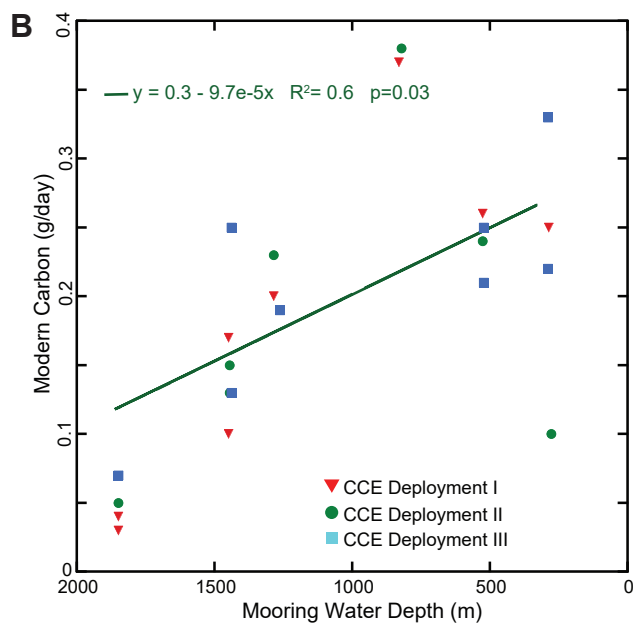
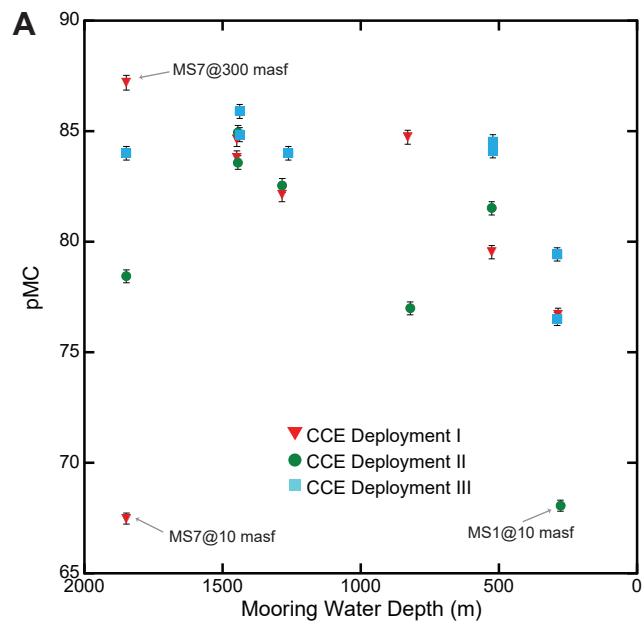
¹Deployment II (April–October 2016); Deployment III (October 2016 – April 2017)

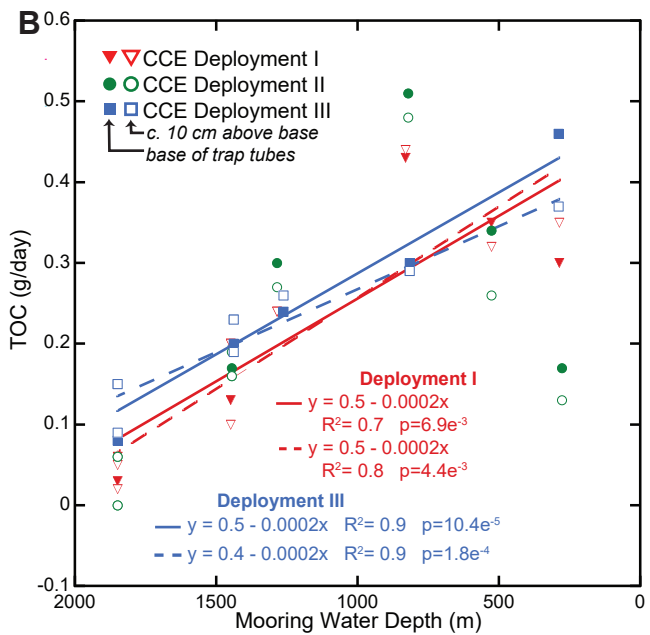
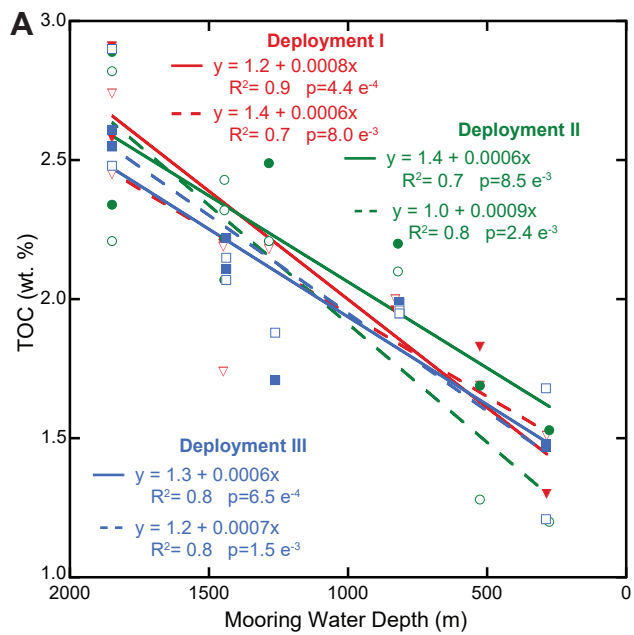


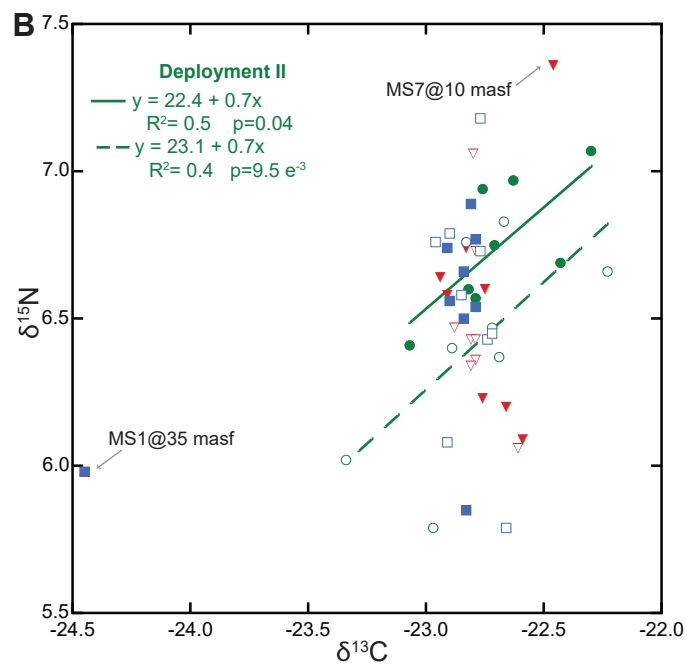
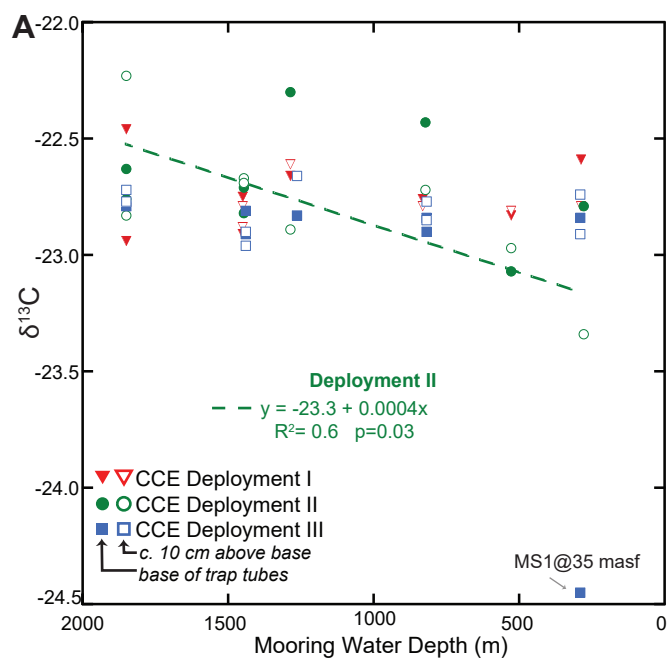
A**B**

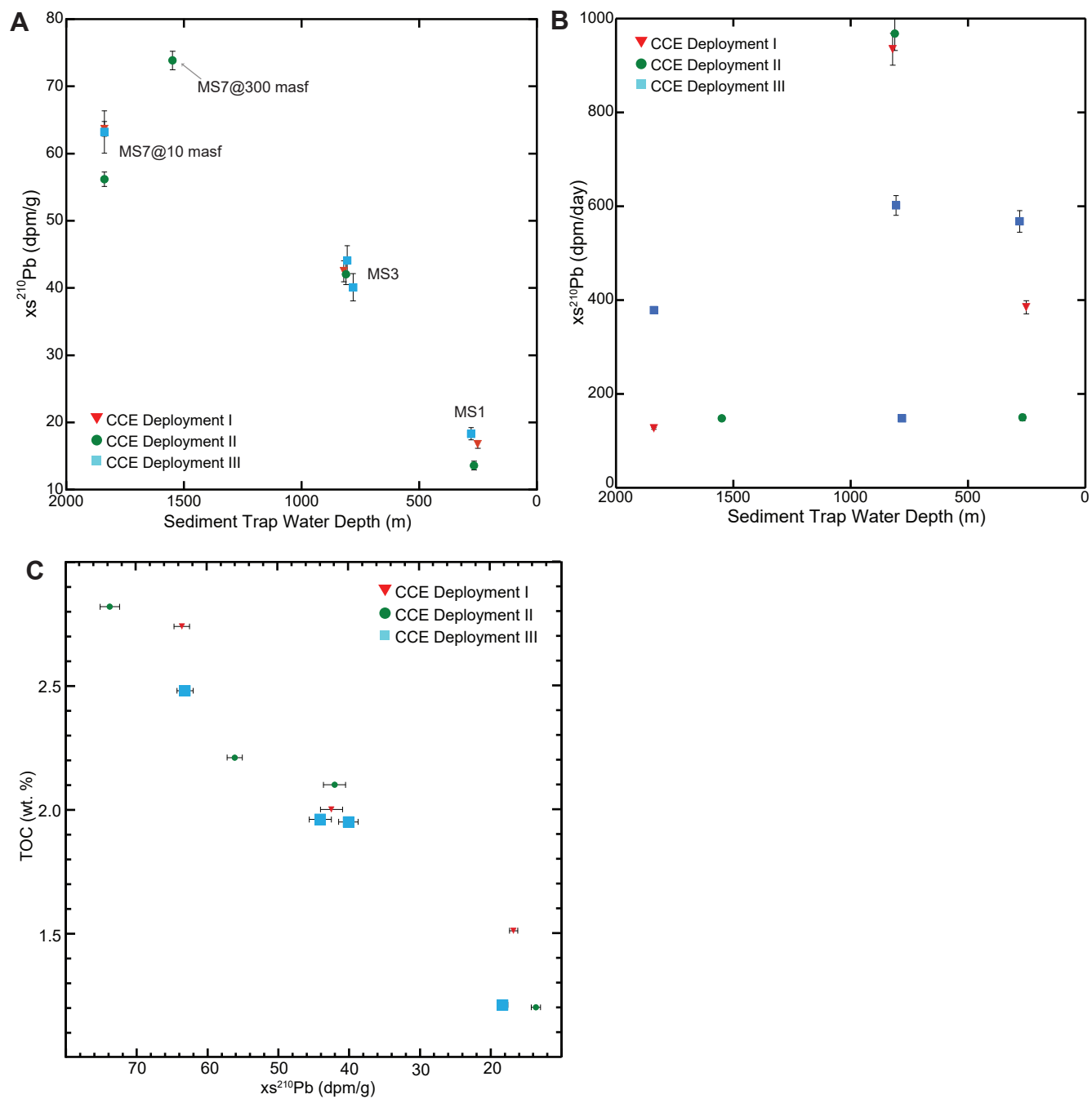


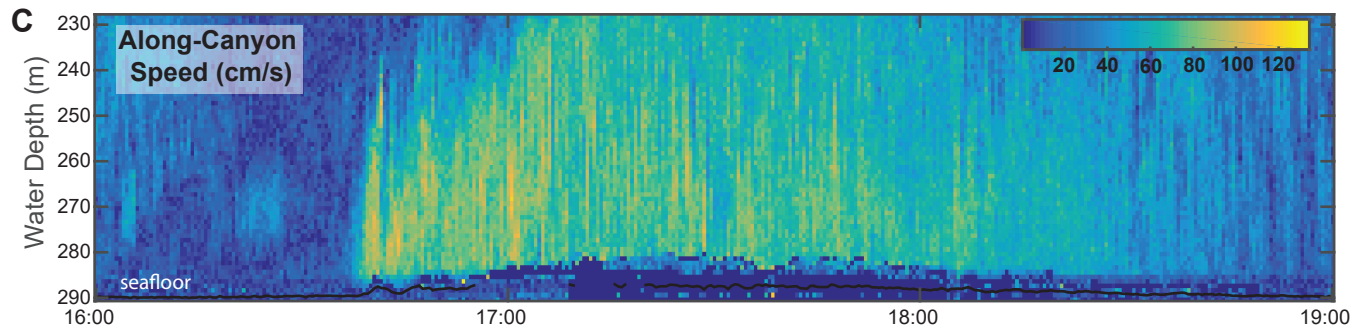
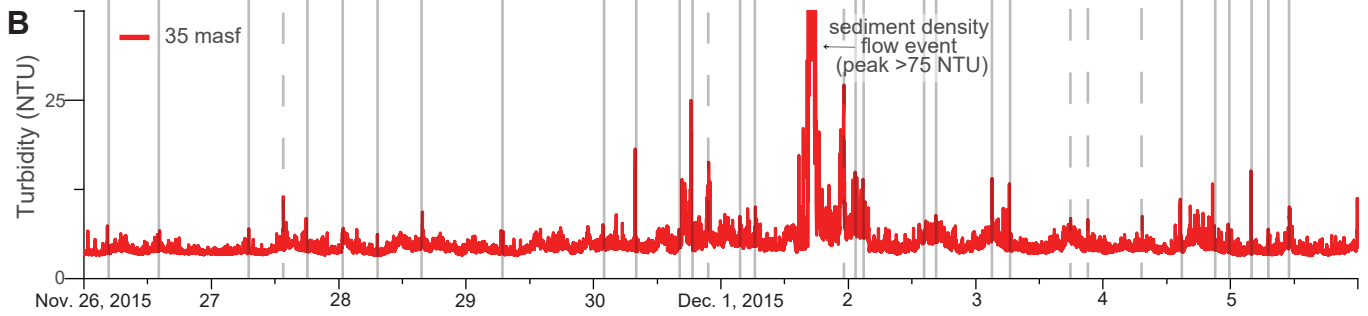
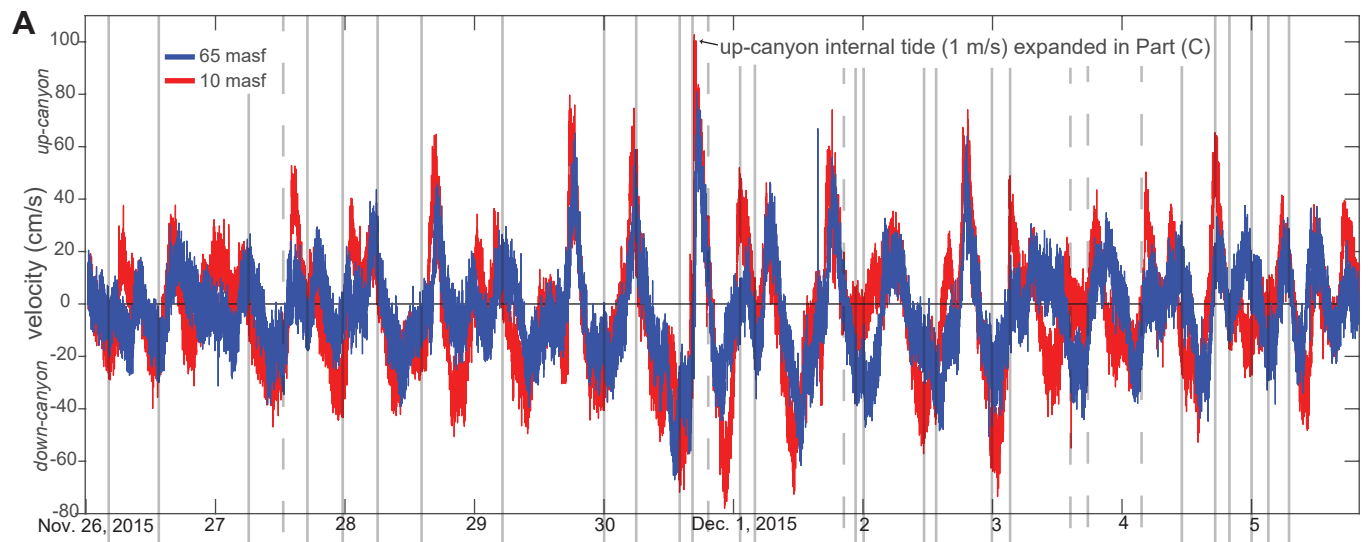


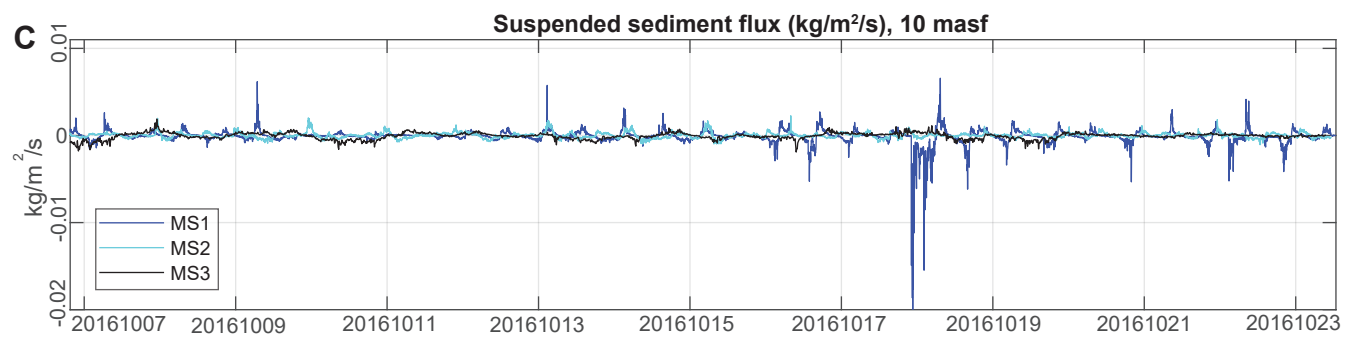
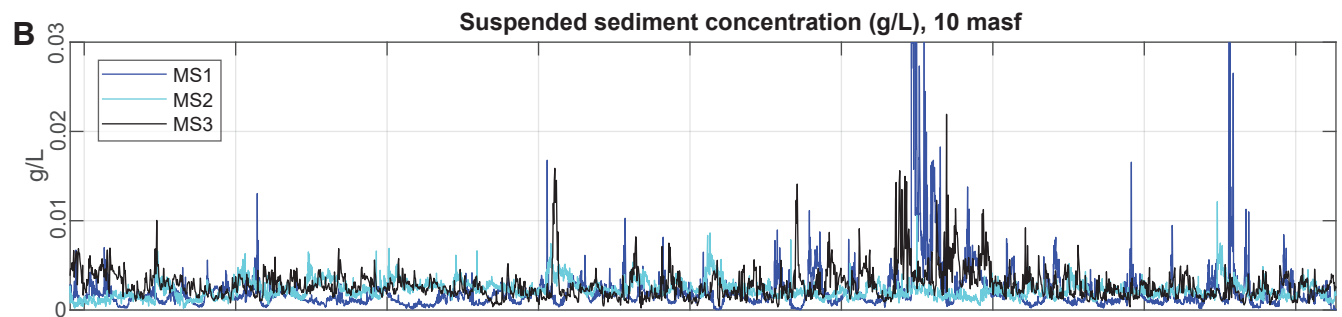
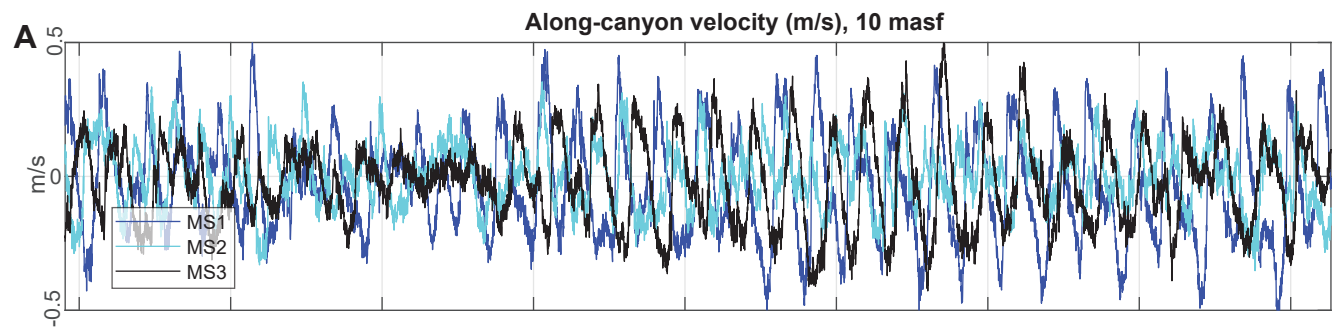


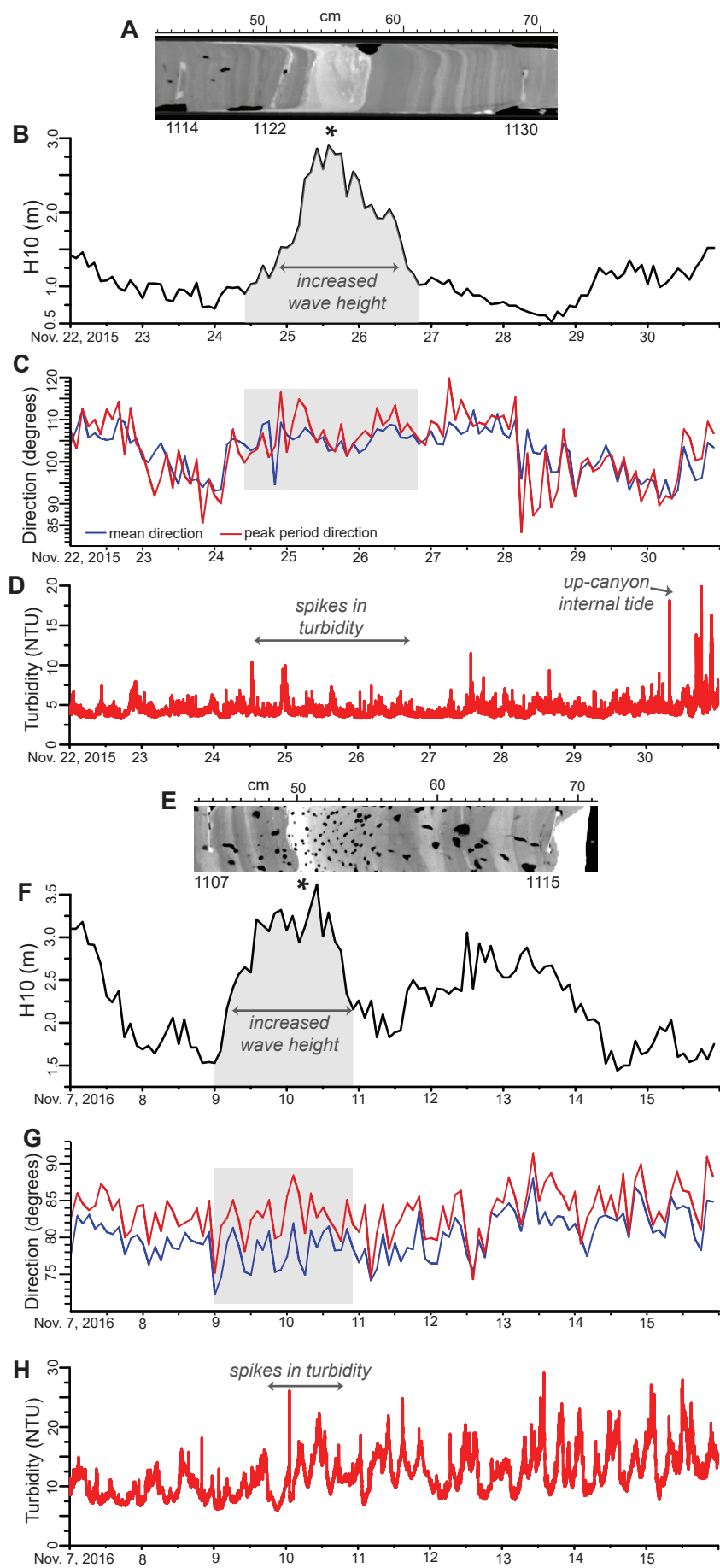


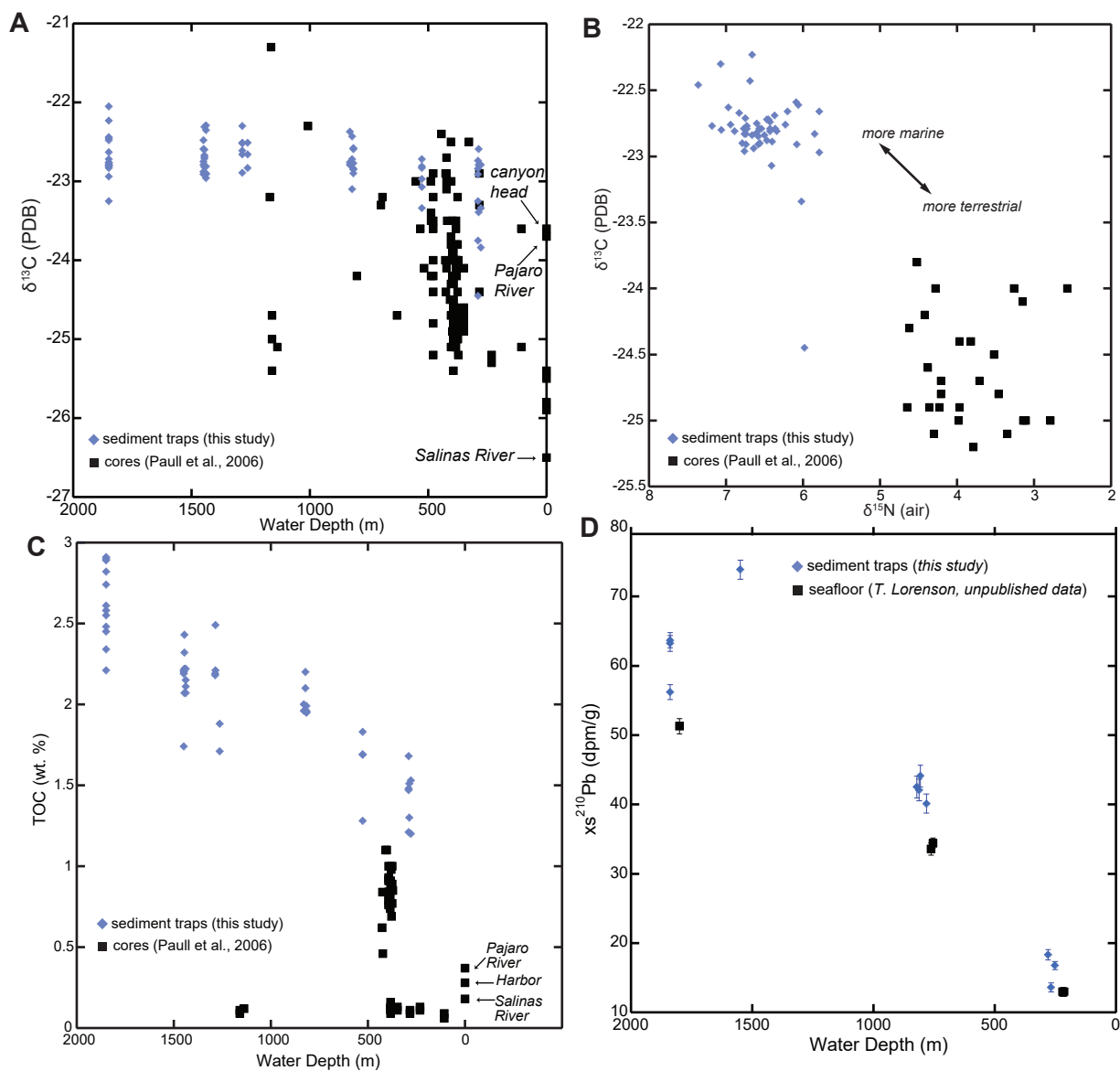


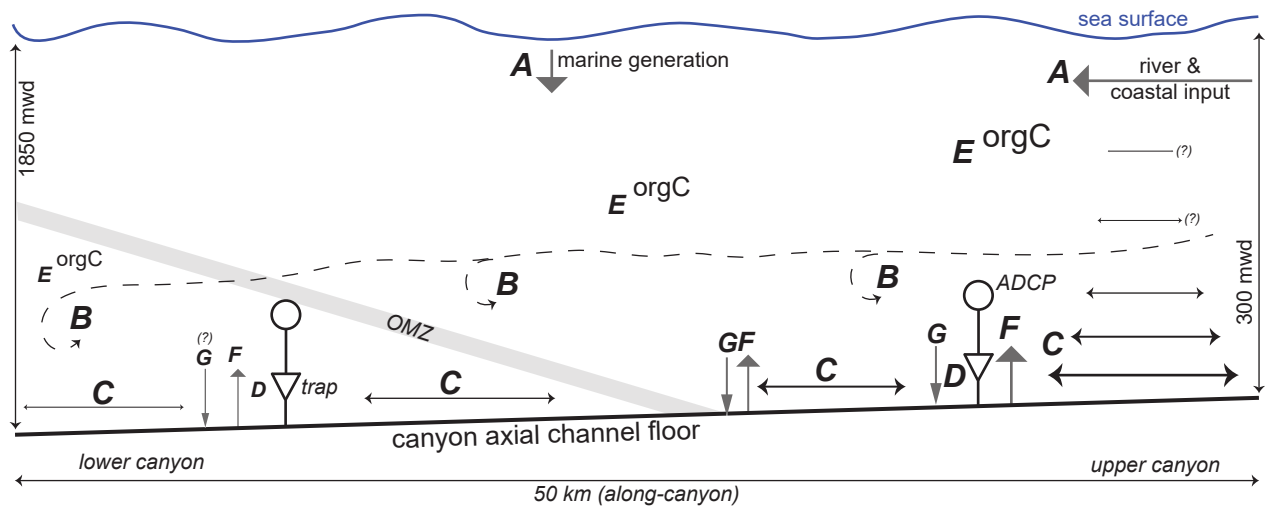












- A** sources of organic carbon - including marine & terrestrial
B along-canyon mixing (dashed) - isotopes & pMC
C internal tide transport of sediment
 - increases towards seafloor & up-canyon
D trap accumulation - rate decreases down-canyon

- E** rate of organic matter delivery to near-seafloor traps
 - decreases down-canyon with sediment flux
F internal tide resuspension of sediment and organic carbon
 from canyon floor and walls - decreases down-canyon
G organic carbon specific burial efficiency
 - low compared to trap capture

Supplementary Table 1. Laser particle grain size summary.

Sediment Trap Sample	Background Sediment Intervals (cm) ¹	D[4,3] (μm) ²	d0.1 (μm) ³	d0.5 (μm) ⁴	d0.9 (μm) ⁵
MS1_AST35m_20161006	15, 16, 20-21, 35-66, 70-76	44.0	4.1	22.6	99.1
MS2_AST10m_20151005	0-76	32.6	3.8	17.1	69.5
MS3_AST10m_20151005	30-86	36.8	3.9	16.9	72.2
MS4_AST10m_20151007	40-56, 75-91	30.2	3.8	15.2	67.2
MS5_AST11m_20151020	45-66	27.7	3.5	13.7	60.1
MS5_AST74m_20151020	0-16, 65-86	29.8	3.4	14.0	66.9
MS7_AST10m_20151027	0-1, 9-22, 79-85	29.5	3.4	14.0	69.0
MS7_AST300m_20151027	0-9	27.2	3.5	13.7	62.8
MS1_AST10m_20160404	10-91	53.3	4.4	27.1	120.8
MS2_AST10m_20150407	0-91	37.9	3.8	18.1	79.9
MS3_AST10m_20150407	0-86	37.8	4.1	16.4	75.1
MS4_AST10m_20150408	5-96	37.7	3.7	15.4	77.4
MS5_AST11m_20150408	30-91	32.0	3.9	14.5	68.9
MS5_AST74m_20150408	0-16, 25-71	31.3	3.7	15.0	70.9
MS7_AST10m_20150420	all (<i>see Table 1</i>)	39.7	3.8	15.0	91.7
MS7_AST300m_20150420	0-16	37.7	3.9	14.4	83.9
MS1_AST10m_20161006	15-76	51.0	4.3	26.7	112.1
MS1_AST35m_20161006	0-11	50.1	3.9	23.8	122.8
MS3_AST10m_20161006	25-96	31.6	3.7	16.6	70.6
MS3_AST35m_20161006	10-86	29.6	3.7	16.1	65.6
MS4_AST10m_20161007	0-26, 40-76	33.0	3.7	15.1	72.8
MS5_AST11m_20161007	25 - 85	29.4	3.7	14.7	66.5
MS5_AST74m_20161007	10-11, 40-81	29.8	3.7	15.0	67.3
MS7_AST10m_20161019	0-56, 65-66	43.5	3.9	15.8	95.0
MS7_AST300m_20161019	0-11, 15-21	25.3	3.7	13.2	54.8

¹measured from top of Anderson sediment trap liner tube sediment²volume mean diameter of grain³10th percentile diameter of grain⁴median diameter of grain⁵90th percentile diameter of grain

Supplementary Table 2. Radiocarbon analyses.

Sediment Trap Sample	Interval (cm) ¹	$\delta^{13}\text{C}$ (PDB)	pMC ²	\pm pMC ²	Apparent modern carbon flux (g/day) ³	Apparent modern carbon flux (g/m ² /day) ³
MS1_AST35m_20151006	78-79	-23.4	76.7	0.3	0.2	4.9
MS2_AST10m_20151005	79-80	-23.3	79.5	0.3	0.3	5.2
MS3_AST10m_20151005	88-89	-22.4	84.7	0.3	0.4	7.5
MS4_AST10m_20151007	94-95	-22.5	82.1	0.3	0.2	3.9
MS5_AST11m_20151020	70-71	-22.6	84.6	0.3	0.2	3.4
MS5_AST74m_20151020	89-90	-22.5	83.8	0.3	0.1	2.0
MS7_AST10m_20151027	86-87	-23.3	67.5	0.3	0.0	0.8
MS7_AST300m_2015102	8-9	-22.1	87.2	0.3	0.0	0.5
MS1_AST10m_20160404	92-93	-23.8	68.1	0.3	0.1	2.0
MS2_AST9m_20160407	93-94	-22.7	81.5	0.3	0.2	4.9
MS3_AST9m_20160407	88-89	-23.1	77.0	0.3	0.4	7.5
MS4_AST10m_20160408	95-96	-22.5	82.6	0.3	0.2	4.6
MS5_AST11m_20160408	89-90	-22.3	85.0	0.3	0.2	3.1
MS5_AST74m_20160408	73-74	-22.6	83.6	0.3	0.1	2.7
MS7_AST300m_2016042	17-18	-22.4	78.5	0.3	0.0	0.9
MS1_AST10m_20161006	76-77	-23.3	79.4	0.3	0.3	6.7
MS1_AST35m_20161006	12-13	-23.8	76.5	0.3	0.2	4.4
MS3_AST10m_20161006	94-95	-22.6	84.5	0.3	0.3	5.1
MS3_AST35m_20161006	88-89	-22.6	84.1	0.3	0.2	4.2
MS4_AST10m_20161007	79-80	-22.5	84.0	0.3	0.2	3.9
MS5_AST11m_20161007	77-78	-22.4	84.9	0.3	0.3	5.1
MS5_AST74m_20161007	75-76	-22.3	85.9	0.3	0.1	2.6
MS7_AST10m_20161019	64-65	-22.5	84.0	0.3	0.1	1.3

¹measured from top of Anderson sediment trap liner tube sediment²pMC: percent modern carbon³calculated using averaged apparent sediment flux (g/day) in Table 1 and TOC (wt.%) in Table 4

Supplementary Table 3. Organic carbon content and stable isotope analyses.

Sediment Trap Sample	Interval (cm) ¹	Lab #	$\delta^{13}\text{C}$ (PDB)	$\delta^{15}\text{N}$ (air)	C/N atomic	TOC ² (wt. %)	TOC (g/day) ³	TOC (g/m ² /day)	Total N (wt. %)
MS1_AST35m_20151006	64-65	3502	-22.6	6.1	8.6	1.3	0.3	6.0	0.2
MS1_AST35m_20151006	74-75	3503	-22.8	6.7	8.7	1.5	0.3	7.0	0.2
MS2_AST10m_20151005	60-61	3510	-22.8	6.7	8.5	1.8	0.3	7.0	0.3
MS2_AST10m_20151005	70-71	3511	-22.8	6.4	8.5	1.7	0.3	6.4	0.2
MS3_AST10m_20151005	73-74	3517	-22.8	6.2	8.6	2.0	0.4	8.6	0.3
MS3_AST10m_20151005	83-84	3518	-22.8	6.4	8.6	2.0	0.4	8.8	0.3
MS4_AST10m_20151007	87-88	3523	-22.7	6.2	8.5	2.2	0.2	4.8	0.3
MS4_AST10m_20151007	92-93	3524	-22.6	6.1	8.5	2.2	0.2	4.8	0.3
MS5_AST11m_20151020	65-66	3527	-22.8	6.6	9.0	2.2	0.2	4.0	0.3
MS5_AST11m_20151020	94-95	3528	-22.8	6.4	8.9	2.2	0.2	3.9	0.3
MS5_AST74m_20151020	80-81	3536	-22.9	6.6	9.0	2.2	0.1	2.6	0.3
MS5_AST74m_20151020	90-91	3537	-22.9	6.5	9.0	1.7	0.1	2.1	0.2
MS7_AST10m_20151027	78-79	3542	-22.5	7.4	7.9	2.9	0.1	1.2	0.4
MS7_AST10m_20151027	84-85	3543	-22.8	7.1	8.9	2.7	0.1	1.1	0.4
MS7_AST300m_20151027	1-2	3544	-22.9	6.6	8.9	2.6	0.0	0.5	0.3
MS7_AST300m_20151027	6-7	3545	-22.8	6.3	8.7	2.4	0.0	0.5	0.3
MS1_AST10m_20160404	80-81	3553	-22.8	6.6	8.8	1.5	0.2	3.4	0.2
MS1_AST10m_20160404	90-91	3554	-23.3	6.0	9.3	1.2	0.1	2.6	0.2
MS2_AST9m_20160407	80-81	3563	-23.1	6.4	9.0	1.7	0.3	6.8	0.2
MS2_AST9m_20160407	90-91	3564	-23.0	5.8	8.9	1.3	0.3	5.1	0.2
MS3_AST9m_20160407	71-72	3572	-22.4	6.7	8.7	2.2	0.5	10.1	0.3
MS3_AST9m_20160407	80-81	3573	-22.7	6.5	8.8	2.1	0.5	9.7	0.3
MS4_AST10m_20160408	82-83	3582	-22.3	7.1	8.6	2.5	0.3	6.0	0.3
MS4_AST10m_20160408	92-93	3583	-22.9	6.4	8.8	2.2	0.3	5.3	0.3
MS5_AST11m_20160408	77-78	3589	-22.7	6.7	8.9	2.1	0.2	3.3	0.3
MS5_AST11m_20160408	87-88	3590	-22.7	6.8	8.9	2.4	0.2	3.9	0.3
MS5_AST74m_20160408	60-61	3597	-22.8	6.6	8.8	2.2	0.2	3.1	0.3
MS5_AST74m_20160408	70-71	3598	-22.7	6.4	9.0	2.3	0.2	3.3	0.3
MS7_AST10m_20161420	B1*	3599	-22.8	6.9	9.0	2.3	N/A	N/A	0.3
MS7_AST10m_20161420	B6*	3600	-22.8	6.8	8.9	2.2	N/A	N/A	0.3
MS7_AST300m_20160420	10-11	3603	-22.6	7.0	8.8	2.9	0.1	1.2	0.4
MS7_AST300m_20160420	15-16	3604	-22.2	6.7	8.8	2.8	0.1	1.1	0.4
MS1_AST10m_20161006	60-61	3610	-22.8	6.5	9.0	1.5	0.5	9.2	0.2
MS1_AST10m_20161006	70-71	3611	-22.9	6.1	8.8	1.2	0.4	7.5	0.2
MS1_AST35m_20161006	1-2	3612	-24.4	6.0	9.4	1.5	N/A	N/A	0.2
MS1_AST35m_20161006	9-10	3613	-22.7	6.4	8.9	1.7	N/A	N/A	0.2
MS3_AST10m_20161006	80-81	3622	-22.9	6.6	8.9	2.0	0.3	5.9	0.3
MS3_AST10m_20161006	90-91	3623	-22.8	6.7	8.8	2.0	0.3	5.9	0.3
MS3_AST35m_20161006	70-71	3631	-22.8	6.7	8.8	2.0	0.3	6.0	0.3
MS3_AST35m_20161006	80-81	3632	-22.8	6.6	8.8	1.9	0.3	5.8	0.3
MS4_AST10m_20161007	61-62	3639	-22.8	5.8	8.3	1.7	0.2	4.8	0.2
MS4_AST10m_20161007	71-72	3640	-22.7	5.8	8.4	1.9	0.3	5.3	0.3
MS5_AST11m_20161007	70-71	3648	-22.8	6.9	8.9	2.1	0.2	4.6	0.3
MS5_AST11m_20161007	78-79	3649	-22.9	6.8	8.9	2.1	0.2	4.6	0.3
MS5_AST74m_20161007	69-70	3656	-22.9	6.7	9.0	2.2	0.2	4.0	0.3
MS5_AST74m_20161007	76-77	3657	-23.0	6.8	9.0	2.2	0.2	3.9	0.3
MS7_AST10m_20161019	57-58	3663	-22.8	6.5	8.9	2.6	0.2	3.1	0.3
MS7_AST10m_20161019	62-63	3664	-22.7	6.4	9.0	2.5	0.1	3.0	0.3
MS7_AST300m_20161019	15-16	3668	-22.8	6.8	8.8	2.6	0.1	1.6	0.3
MS7_AST300m_20161019	20-21	3669	-22.8	7.2	8.8	2.9	0.1	1.7	0.4

¹measured from top of Anderson sediment trap liner tube sediment²TOC: total organic carbon³calculated using averaged apparent sediment accumulation rate from Table 1

Supplementary Table 4. ²¹⁰Pb analyses.

Sediment Trap Sample	Interval (cm) ¹	Dry bulk density (g/cm ³)	Total ²¹⁰ Pb (dpm/g)	²²⁶ Ra (dpm/g)	± ²²⁶ Ra (dpm/g)	xs ²¹⁰ Pb (dpm/g)	± xs ²¹⁰ Pb (dpm/g)	xs ²¹⁰ Pb (dpm/day) ³	± xs ²¹⁰ Pb (dpm/day) ³	xs ²¹⁰ Pb (dpm/m ² /day) ³	± xs ²¹⁰ Pb (dpm/m ² /day) ³	¹³⁷ Cs (dpm/g)	± ¹³⁷ Cs (dpm/g)
MS1_AST35m_20151006	74-77	0.91	18.38	1.62	0.09	16.76	0.59	385	14	7700	280	0.12	0.04
MS1_AST10m_20160404	87-90	1.02	15.23	1.64	0.08	13.59	0.65	150	7	3000	140	0.16	0.07
MS1_AST10m_20161006	72-75	0.88	20.21	1.87	0.11	18.34	0.74	568	23	11360	460	0.15	0.05
MS3_AST10m_20151005	86-89	0.75	45.02	2.51	0.19	42.51	1.57	935	34	18700	680	0.06	0.01
MS3_AST10m_20160407	86-89	0.77	44.59	2.50	0.22	42.09	1.56	968	36	19360	720	0.11	0.03
MS3_AST10m_20161006	93-96	0.70	46.78	2.67	0.22	44.10	1.55	662	23	13240	460	0.21	0.02
MS3_AST35m_20161006	86-89	0.71	42.59	2.46	0.20	40.13	1.37	602	21	12040	420	0.06	0.01
MS7_AST10m_20151027	81-84	0.65	67.21	3.52	0.12	63.69	1.10	127	2	2540	40	0.10	0.03
MS7_AST10m_20160420	B9-B11 ²	0.62	59.20	2.98	0.13	56.21	1.09	N/A	N/A	N/A	N/A	0.17	0.07
MS7_AST300m_20160420	12-15	0.63	77.92	4.05	0.16	73.87	1.40	148	3	2960	60	0.13	0.05
MS7_AST10m_20161019	59-62	0.64	66.48	3.25	0.14	63.24	1.14	379	7	7580	140	0.16	0.05

¹ measured from top of Anderson sediment trap liner tube sediment² bulk samples from intervals 9 to 11³ calculated using averaged apparent sediment accumulation rates from Table 1